frontiers | Frontiers in Mechanical Engineering

TYPE Review
PUBLISHED 02 September 2022
DOI 10.3389/fmech.2022.983334

OPEN ACCESS

EDITED BY
Valentin L. Popov,
Technical University of Berlin, Germany

REVIEWED BY
Alexander E. Filippov,
Donetsk Institute for Physics and Engineering, Ukraine
Yijie Jiang,
University of North Texas, United States

*CORRESPONDENCE
Sergej Fatikow,
sergej.fatikow@uni-oldenburg.de

†These authors have contributed equally to this work

SPECIALTY SECTION
This article was submitted to Tribology, a section of the journal Frontiers in Mechanical Engineering

RECEIVED 30 June 2022
ACCEPTED 22 July 2022
PUBLISHED 02 September 2022

CITATION
Mead JL, Klauser W, von Kleist-Retzow F and Fatikow S (2022), Advances in assembled micro- and nanoscale mechanical contact probes. *Front. Mech. Eng* 8:983334. doi: 10.3389/fmech.2022.983334

Advances in assembled micro- and nanoscale mechanical contact probes

James L. Mead†, Waldemar Klauser†, Fabian von Kleist-Retzow† and Sergej Fatikow*

Division of Microrobotics and Control Engineering, Department of Computing Science, University of Oldenburg, Oldenburg, Germany

The micro- and nanoscale characterization and mapping of surface properties and surface behaviour is critical to both physical and biological science. Mechanical contact probes are a critical tool for investigating surface and interface science, and have seen greater development and a diversification in recent years. In particular, mechanical contact probes that have been fabricated from the bottom-up by the assembly of synthesized nano- or microscale materials can provide enhanced functionality and sensitivity over traditional microcantilevers. This work provides an overview of recent developments in the field of assembled micro- and nanoscale mechanical contact probes, with a specific focus on three probe types: colloidal particle probes with high aspect ratio and a high lateral sensitivity, one-dimensional probes comprising of nanotube and/or nanowire deflection elements, and liquid metal-based probes. For each probe type, the state-of-the-art is reviewed, and their assembly, design, functionality and capabilities are discussed. An outlook on the future direction of probe development and potential applications is also given.

KEYWORDS

pick and place, mechanical probe, interfacial interaction, colloidal particle, one dimensional materials, nanowire, liquid metal

1 Introduction

The capability to probe with micro- or even nanoscale spatial precision is essential for the characterization or mapping of, interaction with, modification of, and overall exploitation of the surface, surface properties, and surface behavior of small-scale structures in both physical and biological sciences. The assembly and functionality of the ever-expanding variety of micro- and nanoelectromechanical systems is dependent on the surface properties of their integrated small-scale components (Wang and Madou, 2005; Seo et al., 2020). In biological systems, the micro- and nanoscale surfaces of cells, bacteria, viruses, and proteins dictate how they interact with one another in biological processes, and can be probed to uncover their structure and functionality (Anselme et al., 2010; Khalili and Ahmad, 2015). The ability to understand, modify, and interact with such surfaces is facilitating the development of novel materials and composites

(Arash et al., 2014), ultra-sensitive photo- chemical- and biological detectors (Holzinger et al., 2014), energy harvesters (Gong et al., 2020), cell-specific drug delivery approaches (Fischer et al., 2009), nanoprecise surgical tools, and innovative cancer treatments (Cross et al., 2008).

Physical probes that measure the force between their tip and a surface of interest via mechanical transduction is now an extensively applied technological approach to surface investigation (Bhushan, 2005). Ubiquitous application of mechanical probes can be attributed to the overwhelming success of the atomic force microscope (AFM). Surface force measurement can be used to map the topography of the surface, extract elastic parameters, but also to measure adhesion and friction, and subsequently to elucidate surface interactions and chemical properties. Surface forces can also be used to pick-up, move, and/or deposit nanoparticles or materials on a surface, or to modify the surface through wear. As a mechanical probe is brought in contact with a surface, the surface forces interacting with the probe cause it to mechanically deform (Israelachvili, 2011). The deformation is then read-out using various approaches, including but not limited to the optical beam deflection approach (OBDA), interferometry, imaging via optical or electron microscopy, and strain sensing via resistance measurement (Dukic et al., 2015; Rossi et al., 2017).

The vast majority of conventional mechanical probes are fabricated in-batch via "top-down" lithography-based approaches (Albrecht et al., 1990). Lithography, as a standard industrial process, has enabled a vibrant industry of sellers offering low-cost mechanical probes with application-specific designs. Nevertheless, some inherent limitations persist in the top-down fabrication of mechanical probes. These limitations include:

- The existence of surface defects. Industrial lithography processes utilize etching steps to selectively remove material. After chemical wet etching or reactive ion etching, defects and adsorbents remain at the surface (Oehrlein, 1989).
- Limited material composition. Industrial lithography processes are based on the processing of doped Si wafers. If a structure made from an alternative material is required, it must be deposited onto the Si substrate as a secondary process and lifted off (Hsieh and Wu, 2007).
- Limited geometrical shapes. Deep reactive-ion etching is a highly anisotropic etching processes that permits the formation of holes and trenches with high-aspect ratios. Nevertheless, it is difficult to produce side-walls with zero tapering (Laermer et al., 2020). The fabrication of small-scale suspended structures with complex non-tapered geometry is therefore difficult.

These limitations in turn can restrict the functionality of the final probe depending on its aim and design. For example:

- When aiming to develop a mechanical probe with extremely high force sensitivity, its dimensions must be further miniaturized. Specifically, the lateral dimensions of a cantilever probe must be reduced in order to maximize deflection induced by an applied end force (Moser et al., 2013). However, as surface-to-volume ratio of the probe structure increases, its surface condition begins to dominate its mechanical behavior (Poggio, 2013). The surface defects remaining after the etching process facilitate mechanical dissipation during resonance, increasing the fundamental noise associated with its deflection, and therefore limiting its detectable force resolution (Cleland and Roukes, 2002).
- To fundamentally quantify the interfacial interactions between a probe tip and a surface (surface forces) it is essential that the composition and structure of the probe tip surface is well defined (Israelachvili, 2011). Additionally, being able to probe with a range of specific or standard tip materials can be a powerful approach to isolating particular interfacial interactions (i.e. hydrophilic or hydrophobic surfaces) or to clarify how a surface interacts under different conditions. The reactive surface of 'top-down' fabricated Si probes therefore do not necessarily provide an ideal surface for fundamental study (Maszara et al., 1988). The sputtering of thin films onto the tip of Si probes is a common practice, but precisely controlling the final structure of the deposited film is difficult (Babcock et al., 1994).
- To relate a measured force to material-specific adhesion force or energy per unit area parameters, the contact area and average contact separation distance between the probe tip and surface must be determined (Rabinovich et al., 2000; Jacobs and Martini, 2017). Here, either a perfectly hemispherical tip or an atomically smooth crystal plane is ideal. However, most 'top-down' fabricated Si probes have relatively poorly defined tip curvatures as etching processes are not perfectly anisotropic and do not provide atomic precision.

In reverse to the approach of top-down fabrication, mechanical probes can be fabricated 'bottom-up' by the assembly of nano- or microscale structures that have been synthesized molecule-by-molecule (Pu and Hu, 2022). Such synthesized structures are almost unrestricted in their composition, or may be designed with composition gradients, can have atomically smooth facets, with very low defect densities, and with well-defined surface termination (Ozin and Arsenault, 2015; Bohidar and Rawat, 2017). The size and shape of such structures are also unrestricted; they can be 0D, 1D, 2D, can be synthesized in arrays, or produced as perfect spheres with exact diameters. In this introduction, we consider three different bottom-up synthesized micro- and nanomaterials, and discuss how they can be assembled into a mechanical probe in order to

provide improved functionality over conventional top-down fabricated probes.

To understand how a synthesized nano- or microscale component can be exploited within a mechanical probe, it is useful to consider what specific functions must the probe carry out, and what structural features or 'elements' are responsible for providing the functionality. The first function of a mechanical probe is to interact with the surface of interest. Typically, this is done by bringing the element in contact with the surface, forming an interface. This function is typically facilitated by a "tip", which we can more generally refer to as a "sensing element". The second function of a mechanical probe is for it to deform or deflect in a way that can be read-out. For cantilever probes typically used in AFM, interaction with the tip induces a deflection in the main cantilever, which has a reflective top surface that permits its deflection to be detected by a optical beam deflection approach. We can refer to this main cantilever as a "deformation" or "deflection element". Deformation of this element must be detectable for the functionality of the probe. Mechanical probes can be designed in a way whereby the sensing and deformation functionality are performed by separate structural features or elements, or both functions can be performed by a single element.

Colloidal particles (CPs) are solid particles with sizes ranging from 10s of nanometers to several microns, and are now commonly integrated into mechanical probes as a sensing element. CPs can be synthesized from a large variety of materials (Reiss et al., 2009; Zimmermann et al., 2020; Chighizola et al., 2021). Their surface interactions can also be tuned precisely by chemical means. Furthermore, synthesis can be achieved with a size polydispersity of less than 3% (Lu and Weitz, 2013). When used as the sensing element of a mechanical probe, CPs can therefore offer a contact surface with tailorable composition, surface chemistry, shape, and diameter. To do this, CPs are typically deposited and fastened to the end of a tipless etched microcantilever, forming a CP-probe. In this way, the CP substitutes the poorly defined geometry and composition of a standard etched Si tip. Positioning and fastening of CP to microcantilevers has been achieved via a variety of means (Schmutz et al., 2008; Indrieri et al., 2011; Brissinger et al., 2013; Mark et al., 2019; Zimmermann et al., 2019). Fabricating a set of CP-probes with varying composition or diameter can permit the methodical investigation of fundamental interface interactions. Also, the precise spherical shape of CPs permits the use of well-established adhesion-contact models (Johnson et al., 1971; Derjaguin et al., 1975; Tabor, 1977; Maugis, 1992; Fischer-Cripps, 2000), permitting quantification of surface area-specific parameters. However, these contact models were developed for perfectly smooth surfaces. Yet, surface roughness can have a major influence on adhesion in general (Jiang and Turner, 2016; Thimons et al., 2021), causing adhesion hysteresis e.g. for soft materials (Dalvi et al., 2019), and drastically reducing adhesion between rough solid objects with a high Young's modulus (Fuller und Tabor 1975). Approaches to incorporate the influence of roughness into contact mechanic models have been developed by Fuller and Tabor (Fuller und Tabor, 1975), Greenwood and Williamson (Greenwood et al., 1966), and Rumpf (Rumpf, 1974), among others. These models approximate the surface roughness by spherical asperities. Later, Rabinovich et al. (Rabinovich et al., 2000) used the root mean square roughness and the average lateral distance between asperities rather than only the asperity radius. Their model leads to more realistic results when compared with AFM experiments (Rabinovich et al., 2000). Additionally, fractals have been used to characterize surface roughness (Majumdar und Bhushan 1990; Archard 1957; Persson 2007) predicting an exponential growth of load with increasing indentation. This relationship has been proven experimentally for randomly rough surfaces in a surface force apparatus (Benz et al., 2006; Lorenz und Persson 2009). In the end, the choice of the appropriate contact model depends highly on the surface characteristics and application case. The influence of roughness should be kept in mind not only during the analysis of CP-based experiments, but also for experiments based on one-dimensional materials and liquid metals as described below.

One-dimensional (1D) nanomaterials such as nanowires (NWs) and nanotubes (NT) are now regularly used to "decorate" the tips of conventional mechanical probes, and can also act as highly compliant deflection elements (Wong et al., 1998). Carbon nanotubes (CNTs) and boron nitride nanotubes with varying shell numbers and lengths can be synthesized, providing high-aspect ratio structures with tailorable bending stiffness and effective tip diameter (Zhou et al., 2002). NWs can be synthesized with a range of compositions, or with segmented composition, various crystal structures, with specific surface termination, wide range of diameters, with negligible tapering (Duan and Lieber, 2000; Dasgupta et al., 2014). Due to their single crystal structure containing an extremely low number of defects, NW and NTs typically exhibit fracture strengths many orders of magnitude higher than their bulk counterparts (Wang et al., 2015). CNTs also exhibit high wear resistance and are chemically inert (Wilson and Macpherson, 2009). The unique properties of 1D materials therefore make them well suited for use as a sensing element for mechanical probes. For example, CNTs are now regularly cantilevered off the end of the Si tip of conventional microcantilevers for topographic surface scanning applications. Here, the high aspect ratio of the wear resistant tip replacement allows it to reach into pits and scan side walls (Akita et al., 2000). In environments where etched Si tips tend to be modified through chemical reactions, inert CNT tips have also been found to outperform. The decoration of tips with CNTs has been achieved by growing in place using chemical vapor deposition (CVD) or transferred via nanorobotic pick-and-place methods, using a bias voltage for alignment assistance, and electron beam induced deposited carbon (EBiD) for robust fastening (Nguyen et al., 2005).

Aside from performing the role of a sensing element, NWs are also particularly well suited to act as a deflection element when their diameter is carefully chosen. Specifically, the deflection of cantilevered NWs with sufficiently large diameters have been detected using interferometry (Rossi et al., 2017), scanning electron microscopy (SEM) (Mead et al., 2018), optical microscopy-based fringe pattern analysis (Mead et al., 2020), and from optical micrographs (Yibibulla et al., 2022). Such NWs still exhibit extremely large aspect ratios, and hence provided orders of magnitude lower bending stiffness than conventional top-down fabricated probes. Additionally, the atomically smooth crystalline surface of facetted NWs can also be used as the contact surface (Tsivion et al., 2012). By orientating a NW's axis parallel to the surface of interest, bringing into contact, and subsequently peeling from the substrate; the NW can act as both the sensing and deflecting element (Mead et al., 2020). The geometrically well-defined planar contacting facet of the NW forms an interface with the surface of interest, with the average separation distance approximated using a standard rough plate contact model (Greenwood et al., 1966; Greenwood, 1997).

Liquid metal droplets can also be used to form both the sensing and deformation element of mechanical probes. Liquid metal droplets can be formed from various compositions, including Gallium based liquids (e.g. EGaIn or Galinstan) or mercury. Whereas the use of Hg is decreasing more and more because of its toxicity. The diameter of liquid metal droplets can be tailored by top-down processes such as using a blender (Tevis et al., 2014) and a simple syringe (Natalia Sobczak et al., 2010), or via bottom-up processes such as physical vapor deposition (PVD) (Kleist-Retzow and von, 2021) or by means of controlled electromigration (Kleist-Retzow von et al., 2019b). As the surface tension of the droplets determines its shape, when brought into contact with a substrate, its shape is entirely defined by the surface energies of the interface components (Klauser et al., 2022). After liquid metal spheres are formed with the desired diameter, they can be mounted on a manipulator or cantilever by controlled wetting processes. For this purpose, wetting methods such as electrowetting (Diebold et al., 2017), forced wetting by ion implantation (Kleist-Retzow and von, 2021) or electromigration-induced wetting (Kleist-Retzow von et al., 2019b) can be utilized. Liquid metal probing therefore has benefits over top-down fabricated Si tips by establishing a hard-soft-hard interface for practically abrasion-free contact probing and maximizing the contact area without wear and mechanical deformation (Kleist-Retzow and von, 2021).

As discussed, the most suitable assembly strategy utilized in the bottom-up fabrication of a probe is dependent on the type of micro- or nanoscale structure that is to be integrated. Strategies available for micro- and nanoscale integration can be broadly divided into "grow-in-place" and "grow-and-place" (Kwiat et al., 2013). Grow-in-place strategies involve synthesizing the nano- or microscale structure directly at the desired location. These methods often deposit a catalyst at a location of interest on the probe, followed by deposition-based growth of the structure of interest (Hernández-Vélez, 2006; Cao and Liu, 2008). In contrast, grow-and-place strategies synthesize the structure externally, and then use a secondary assembly step to integrate the structure into the probe (Shi et al., 2016; Pu and Hu, 2022). Parallel assembly methods offer the potential to be upscaled for industrial level fabrication, and therefore can be considered the end goal (Yerushalmi et al., 2007; Wang and Gates, 2009). However, challenges to precisely align and fasten structures remain an issue. In contrast, nanorobotic pick-and-place assembly methods are a serial procedure, which can be sped up with automation, but cannot be expected to achieve the same output as the parallel methods. Nevertheless, pick-and-place assembly procedures can be rapidly developed and applied to the assembly of a large variety of different nano- and microscale materials. They are therefore well suited for the prototyping stage of mechanical probe assembly. In fact, it is pick-and-place strategies that have enabled the initial development of bottom-up fabricated mechanical probes.

From the above examples, that mechanical probes fabricated from the bottom-up *via* the assembly of molecule-by-molecule synthesized micro- and nanoscale materials, both solid and liquid, can provide superior functionality over conventional top-down fabricated probes when considering specific requirements. In this work, we review in Chapter. 2, 3 and 4, three selected bottom-up assembled mechanical contact probe designs. Each probe design is unique and incorporates a different nano- or microscale structure:

- Colloidal particle probes with long supporting pillars, for adhesion measurement and topographic mapping of textured substrates, sidewalls, and for measuring lateral forces.
- One-dimensional mechanical contact probes for topographic mapping, the fundamental characterisation of adhesion and friction behaviour, and surface energy measurement.
- Liquid metal probes for low abrasion contact procedures like contact angle measurement of liquid-solid interfaces and pick and place processes.

The three highlighted probe types help demonstrate the advances in bottom-up fabricated mechanical contact probes and their diverse applications. In each chapter, the state-of-the-art of the specific assembled probe type is reviewed, including their assembly, design, functionality and capabilities. Chapter 5 provides a perspective and future outlook on each probe type, including possible future design improvements and potential application.

2 Colloidal particle probes

Developed by Binnig et al. (Binnig and Gerber, 1986) in 1986, the AFM was first mainly used for imaging of conductive as well

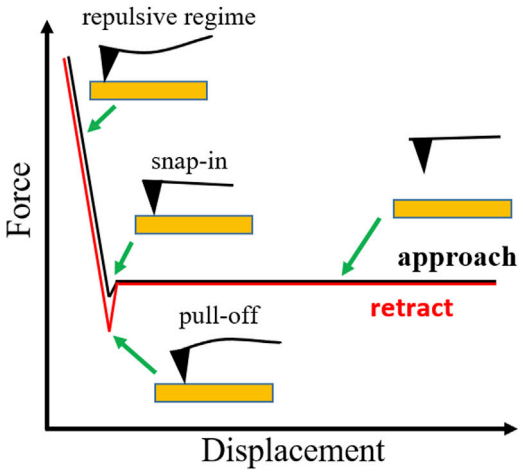

FIGURE 1
Schematic of a force-displacement graph during an AFM force measurement with the characteristic points "snap-in" and "pull-off", the force value at the pull off point corresponds to the adhesion force.

as insulating samples, but has also become a powerful force analysis instrument for the nanoscale during the last decades. For a force measurement the tip attached to the cantilever spring is moved towards the sample in normal direction and the vertical position of the tip and deflection of the cantilever are recorded in a force-distance curve (see Figure 1). The resolution of AFM force measurements can reach the pN range (Butt et al., 2005), and depends on the accuracy of tip-surface distance determination, cantilever properties, and the surrounding medium. Additionally, a variety of instruments based on the AFM has been introduced in the last decades, such as for example the magnetic force microscope and the Kelvin probe microscope to evaluate magnetic and electrostatic properties, respectively. Furthermore, force measurements on biological materials and single molecule experiments with the AFM, e.g. single bond failure tests and polymer stretching, have emerged (Janshoff et al., 2000).

The introduction of the colloidal probe technique (Ducker et al., 1991), where a (in most cases) spherical particle is attached to the cantilever tip, has contributed to the success of the AFM as a force analysis tool. Among other aspects, a smooth sphere of defined radius allows for a higher total force, for evaluation of the interaction between a variety of materials by attaching a sphere with different material properties, and for hydrodynamic force measurements. A variety of materials (e.g. silica spheres, polystyrene (PS) particles, or zirconia particles) are commercially available. Most widely used are silica microspheres and glass particles because of their smooth surface, their availability and the possibility of surface modifications. For a long time, colloidal probe experiments were carried out with particles in the micrometer range (Kappl and Butt, 2002; Helfricht et al., 2017) often attached to tipless cantilevers which did not allow investigation of highly textured surfaces, cavity sidewalls, or friction forces with a high sensitivity. And the existing high aspect ratio cantilever designs (Savenko et al., 2013) did not feature a well-defined tip geometry. However, through the application of high aspect ratio probes decorated with colloidal particles significant advances have been made in these fields during the last years. In the following, first, a brief overview of tip modification methods for the standard fabrication of colloidal probes is presented. Afterwards we focus on recent developments of high aspect ratio probes and their application.

2.1 Particle attachment techniques

Since Ducker et al. (Ducker et al., 1991) and Butt (Butt, 1991) attached silica and glass spheres onto cantilevers in 1991, many types of microspheres have become available (Butt et al., 2005) that can be produced in various ways and attached to cantilevers to form a colloidal probe. Some limiting factors are that the microparticles may be rough or porous, or coated with a layer that helps to prevent aggregation but also changes the surface chemistry and thus not every type of microsphere is equally suited for colloidal probes.

Most widely used are silica microspheres due to their relatively smooth surface with an RMS roughness often below 1 nm (Butt et al., 2005). Amorphous SiO_2 particles are produced by a sol-gel process (Stöber et al., 1968) and commercially available at different sizes and with and without surface modifications. The high melting point of silica (1723°C) makes it difficult to sinter them to cantilevers and they are usually attached with glue. Glass microspheres (Braithwaite et al., 1996; Kokkoli and Zukoski, 2000), usually composed of borosilicate glass and having a similarly smooth surface as the silica ones, are easier to sinter due to their lower melting temperature.

Colloidal particles from various other materials can be produced. Zirconia microspheres are usually fabricated by e.g. annealing of zirconia powder (Pedersen and Bergström, 1999). Alumina (Al_2O_3) microspheres are produced from alumina powder e.g. by melting in a hydrogen-oxygen flame (Nalaskowski et al., 2003). Also, colloidal probes have been fabricated with titanium oxide (TiO_2) (Larson et al., 1993), magnesium oxide (MgO) (Kauppi et al., 2005), and zinc sulfide (ZnS) (Gillies et al., 2005) particles. Additionally, irregular particles and single crystals have been employed for colloidal probes (Finot et al., 1999; Butt et al., 2005) and polymeric microspheres made of polystyrene, polymethylmethacrylate (PMMA) or polyethylene (PE) are commercially available and can be used for colloidal probes as well.

TABLE 1 Particle attachment techniques suitable for colloidal probe fabrication.

References	Technique	Adhesive	Particle Material Limitations	Special Equipment Requirements
Ducker et al. (1991); Mak et al. (2006)	Dual-wire	glue	none	micropipette + micromanipulator
Raiteri et al. (1998); Gan, (2005)	Cantilever moving	glue	none	micromanipulator
Indrieri et al. (2011)	High temperature sintering	none	borosilicate glass only	heatable chamber
Vakarelski and Higashitani, (2006)	Wet-chemical surface assembly	self-assembled silane layer	Au only	none
Sqalli et al. (2002)	Photocatalytic deposition	none	Au only	Sputter coating; evanescent wave illumination
Schmutz et al. (2008)	Tip apex modification for stronger adhesive bonding	glue	none	FIB
Yapici and Zou, (2009)	Mold transfer production of cantilevers with customized dimensions and tip curvature	none	same material as cantilever	Thin film deposition, spin coating

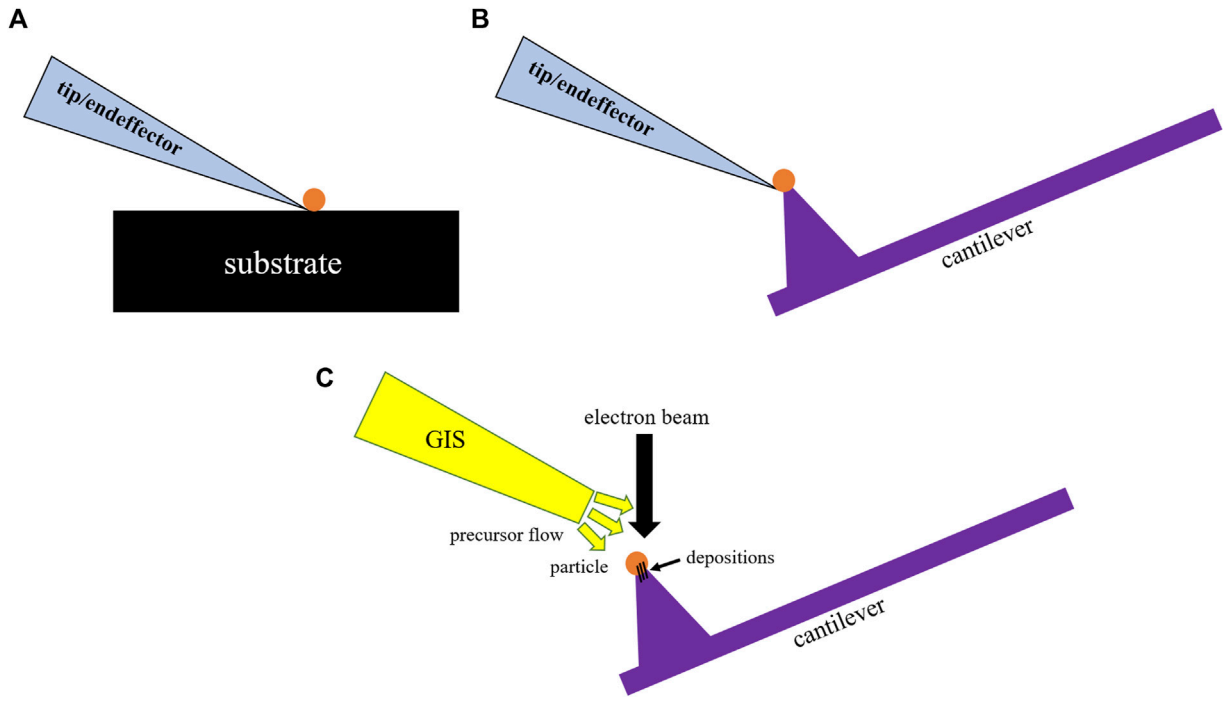

FIGURE 2
Illustration of the principle of a nanorobotically-assisted colloidal probe fabrication process; particle pick up in **(A)**, particle placement at the cantilever tip in **(B)**, and fastening of the particle via electron beam induced deposition (EBiD) in **(C)**.

As mentioned above, different means can be used to attach particles to a cantilever. In the beginning, spheres were often glued to cantilevers using thermoplastics. Alternatively, two component epoxy glues which cross link upon mixing have been used as well (Nigmatullin et al., 2004). However, glue can introduce contaminations and thus particles have also been sintered onto cantilevers: polymer particles can be placed onto a cantilever and heated to close to the glass transition temperature (Karaman et al., 1993). Borosilicate glass particles can be attached to tipless silicon dioxide and poly-silicon cantilevers employing a glycerol layer which holds the particle in place by capillarity. Afterwards, cantilever and particle are

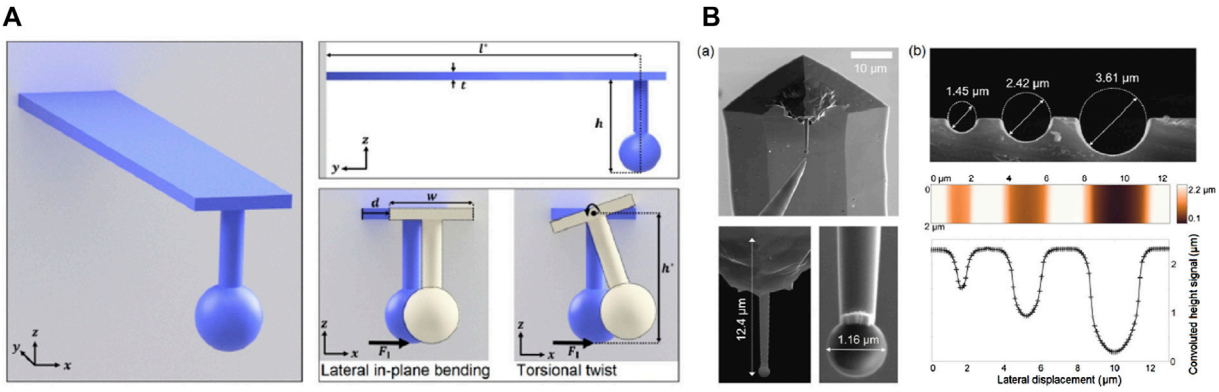

FIGURE 3
(A) Sketch of a cantilever beam with rectangular cross-section and colloidal tip showing the relevant dimensions *t*, *l**, and *h**; **(B)** SEM images of a nanorobotically assembled high aspect ratio colloidal particle probe carrying a 1.16 µm particle at the tip and SEM images as well as AFM height images and profiles of the cavities used to investigate its capability to probe sidewalls. Reprinted with permission from (Zimmermann et al., 2019), Copyright 2018 Springer Nature.

heated to the softening point of the borosilicate glass, which is around ~780°C, for 2 h (Bonaccurso et al., 2002). The glycerol evaporates and contaminations are reduced in this way (Butt et al., 2005).

Table 1 gives an overview of techniques that have been used to attach particles to AFM probes in order to form colloidal probes. Other methods have so far been applied to manufacture modified tips for SNOM and TERS and some of them are at least potentially applicable to colloidal probe fabrication. More details can be found in the works of Gan (Gan, 2005) and Yuan et al. (Yuan et al., 2017). Most techniques are based on adhesives or chemical processes as presented in Table 1. These techniques therefore suffer either from possible contaminations, a lack of reproducibility, or limitations regarding material selection and cantilever geometry (i.e. the low aspect ratio of tipless cantilevers). In recent years, nanorobotic manipulation and handling techniques have helped to avoid these issues and helped to increase the range of possible aspect ratios and the lateral force sensitivity of colloidal probes. Figure 2 shows the principle of such a nanorobotics-assisted particle attachment process. In this way, high aspect ratio colloidal probes have been realized and applied to the investigation of textured surfaces and sidewalls (Zimmermann et al., 2019), friction forces (Zimmermann et al., 2019; Zimmermann et al., 2020), nanoplastic particles (Zimmermann et al., 2020), and the influence of electron beam on adhesion inside the SEM (Zimmermann and Huang, 2019).

2.2 Laterally sensitive colloidal particle probes

For a minimal measurement inaccuracy and maximum lateral force sensitivity, the relative in-plane bending due to a lateral force contribution and thus the ratio of the torque arm stiffness k_t to the in-plane lateral stiffness k_{ip}, of a colloidal probe should be minimized. This can be tackled by adapting the geometry of the probe, and the ratio between k_t and k_{ip} can be estimated from Euler-Bernoulli beam theory (Sader and Green, 2004; Cannara et al., 2006; Chung et al., 2010)

$$k_t/k_{ip} = [2/(3(1+\nu))](t/h^*)^2(l^*/w)^2 \quad (1)$$

with ν representing the Poisson's ratio of the cantilever beam material and h^* representing the torsional arm (see Figure 3A). For a high lateral sensitivity the torque arm stiffness $k_t \sim (wt^3)/(lh^{*2})$ needs to be reduced and thus, either increasing h^* or decreasing t has to be the goal. For most cantilever types the potential for further reduction of the thickness is very limited. This fact makes the extension of the torsional arm length the most viable approach for the task. However, most conventional top-down approaches for particle attachment reach their limits when it comes to fabricating high aspect ratio colloidal particle probes free from adhesive contaminations. Hence, a bottom-up nanorobotic handling approach in combination with focused ion beam milling (FIB) and electron beam induced deposition has been developed showing an improved lateral sensitivity and suitability for the investigation of sidewalls of textured surfaces and lateral forces (Zimmermann et al., 2019) (see Figure 3B).

Further applications of high aspect ratio colloidal particle probes have been the adhesion and friction measurements of e.g. nanoplastic particles (Zimmermann et al., 2020). The nanorobotically assisted fabrication technique described above allows it to attach individual nanocplastic particles from various materials to a probe with a large torque arm (see Figure 4). Thus, adhesion and friction of such particles can be investigated with an

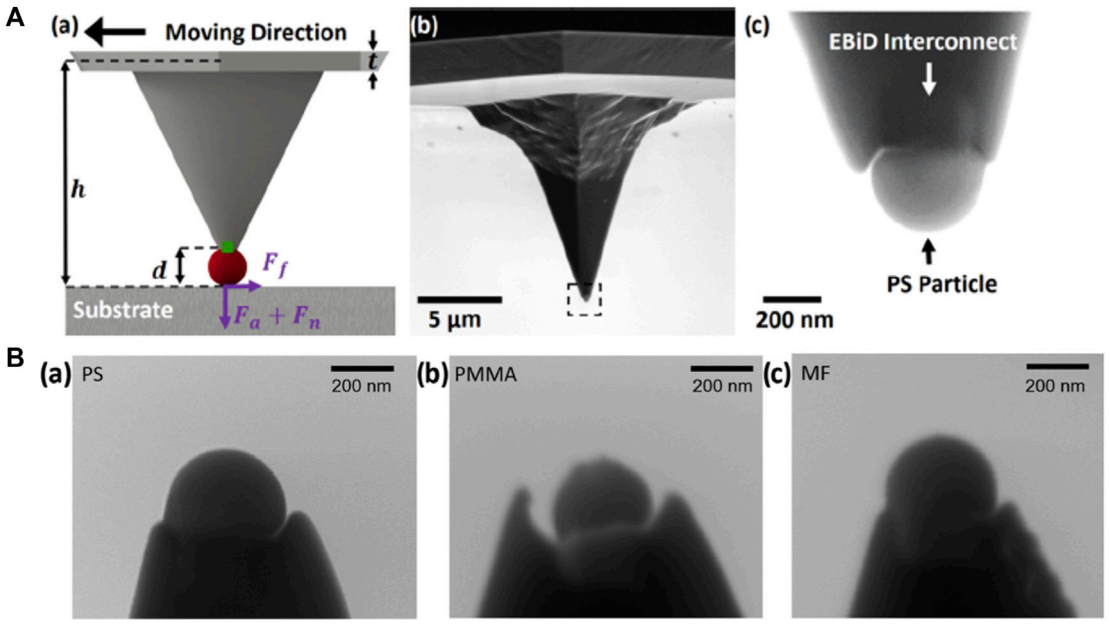

FIGURE 4
(A) Schematic representation of the forces acting on a laterally sensitive colloidal probe during a friction test, and an SEM micrograph of a laterally sensitive colloidal probe with a PS particle that has been fastened to the tip apex via EBiD of a tungsten-based precursor gas; **(B)** SEM micrographs of PS, PMMA, and MF nanoparticles after conducting AFM-based adhesion and friction testing. Reprinted with permission from (Zimmermann et al., 2020) Copyright 2020 American Chemical Society.

improved sensitivity which is vital for e.g. understanding the degradation of micro- and nanoplastics in the environment. The particles can be either synthesized commercially serving as a model case or potentially be particles collected from the environment. So far, measurements with PS, PMMA, and melamine formaldehyde (MF) particles have been carried out.

3 One-dimensional contact probes

The potential to improve the performance of mechanical contact probes by integrating one-dimensional (1D) materials as functional elements was demonstrated by Akita et al. in 2000, where microcantilevers equipped with CNT tips were used to improve topographic surface imaging (Akita et al., 2000). 1D materials, by definition, have cross-sectional dimensions below 100 nm, whilst having aspect ratios over 1,000 (Garnett et al., 2019). 1D materials can be classified into nanotubes, including CNT and boron nitride nanotubes (Kim et al., 2018), and into NW, including, for example, those composed of ZnO, $ZnWO_4$, ZnS, SiC, Si, Al_2O_3 (Jia et al., 2019). In this chapter, we explain why 1D materials are well suited to act as deflection element within a mechanical probe, and conduct a review of the latest corresponding assembled probe designs and their applications.

3.1 The role of one-dimensional deflection elements in probing

The small cross-section and high aspect ratio of 1D materials provides them with an extremely high mechanical compliance. Furthermore, the regular hexagonal lattice of NTs and the single crystal structure of NWs are associated with exceptionally low defect densities, and therefore they can undertake highly deformed shapes without fracturing (Mielke et al., 2004; Wang et al., 2017). The high compliance intrinsic to 1D materials makes them uniquely suited to act as the deflection element within a mechanical probe when aiming to achieve high force sensitivity. This relationship between the mechanical compliance of a probe's deflection element and its force sensitivity can be clarified in a straightforward manner by making some broad assumptions. Consider an arbitrary deflection element, which experiences an applied force, P, causing the element to deflect. If we assume the element deforms elastically, and the deflection remains small, than the induced deflection, δ, is linearly proportional to P by its compliance (or the inverse of its bending stiffness), C; i.e. $\delta = C.P = (1/k)P$ (Megson, 2005). The element's deflection is 'read-out' and converted to a digital signal via a deflection sensor, with the resolution of the final signal dependent on the deflection sensitivity of the sensor, S_δ. Hence, the force sensitivity of a mechanical probe can be most simply defined by:

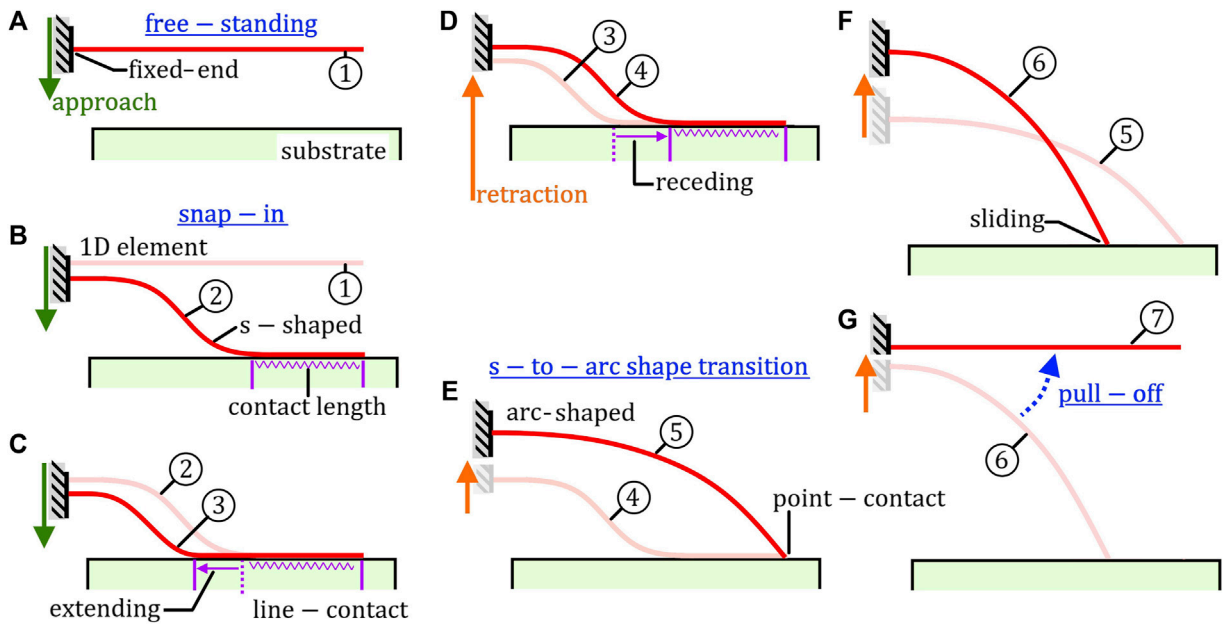

FIGURE 5
Buckling steps exhibited by a parallel-aligned 1D element during approach and retraction from a substrate. Each step is illustrated by the element being shown in states labelled from 1 to 7. **(A)** free-standing 1D element (state 1). **(B)** Snap-in of 1D element, forming a s-shaped profile and a line-contact on the substrate (state 2). **(C)** Extending of line-contact during further approach (state 3). **(D)** Receding of line-contact during retraction (state 4). **(E)** Profile of 1D element transitions from a s-shaped to an arc-shaped profile (state 5). **(F)** Sliding of point-contact at end of 1D element upon further retraction (state 6). **(G)** Pull-off of 1D element upon further retraction, returning to free-standing state (state 7).

$$S_F = (S_\delta C)P \tag{2}$$

In this way, deflection elements with maximized compliance can facilitate the design of probes with higher force sensitivity provided the element remains detectable via the selected read-out strategy.

This simplified definition of force sensitivity utilizes the assumption that when a probe is brought into contact with a surface, that contact occurs at its tip and formes a point contact (or, for example, the circular contact area of a colloidal particle). This assumption is convenient for comparison to traditional microcantilever probes. However, the higher compliance of 1D materials permits them to buckle and conform to surfaces in an unstable manner that is distinct from their conventional counterparts. To clarify this distinct behaviour, it is appropriate to consider the buckling process of a 1D deflection element orientated parallel to the surface of a substrate of interest.

The attachment and detachment process during the approach and retraction of a parallel-aligned 1D deflection element is presented in Figure 5, with Strus et al. providing an in-depth description (Strus et al., 2008; Strus et al., 2009). Each step is illustrated by the element being shown in 'states' labelled from 1 to 7. During approach, the 1D element is free standing, and is brought down towards the surface (state 1, Figure 5A). At a critical separation distance, the 1D element will instantaneously buckle to form an 's' Shape profile, forming a line-contact with the surface (state 2, Figure 5B). This unstable behaviour of a 1D element can be referred to as snap-in. Upon further approach, the 1D element will be permitted to further conform, so that the length of the line contact extends (state 3, Figure 5C). Upon retraction, the 1D element will begin to be peeled off the substrate, with the line contact receding (state 4, Figure 5D). At a critical contact length, the 1D element will instantaneously reconfigure to form arc-shape with its end forming a point contact as shown in (state 5, Figure 5E). The unstable event can be referred to as an s-to-arc-shape transition. Upon further retraction, the 1D element's point contact will tend to slide along the substrate (state 6, Figure 5F). Finally, the element will instantaneously detach from the substrate to again assume a free-standing state (state 7, Figure 5G). This unstable event can be referred to as pull-off.

When used as a deflection element, the complex and unstable buckling behaviour exhibited by 1D material requires alternative approaches to be used for read-out and data evaluation. The common read-out strategies used for microcantilevers typically measure only a single quantity that describes the deformation of the element at a single location over time. For example, the optical beam deflection approach typically measures the slope of deflection at the surface of the microcantilever at a single location

near to its free end (i.e. the position of the laser spot) (Dukic et al., 2015). Similarly, piezoresistive cantilevers measure the average strain experienced over a segment of a microcantilever's top surface (i.e. the region where the piezoresistive layer is formed). For microcantilevers undergoing small deflections, deflection measurement at a single location is sufficient to generate a force-distance curve as the force-deflection relationship remains linearly proportional (Megson, 2005). However, for 1D materials this is not the case. Instead, the deflection at any point along the length of the 1D element is dependent on the length of the 1D segment in contact with the substrate as well as the buckling configuration stable at the given time. Furthermore, the change in slope along the highly deformed profiles of a 1D element is generally large, leading to a non-linear force-displacement relation (Megson, 2005).

In order to effectively evaluate the forces applied to a buckled 1D element without significant uncertainty requires the implementation of a read-out strategy with the capability to observe the entirety of its buckled profile. In addition, one must select appropriate mechanical models that can capture s-shaped and arc-shaped buckling. For example, the Elastica solution provided by Mikata is well suited for describing an elastic rod that undergoes large deformations (Mikata, 2007). In this way, an analytically or numerically modelled buckled profile can then be fitted to closely match the experimentally observed profile. Such approaches have been successfully implemented, for example, by Ke et al., and will be discussed further in the next section (Ke et al., 2010b).

3.2 Nanotube-based contact probes

When examining the state-of-the-art, it becomes clear that the research communities' interest in integrating 1D materials into mechanical contact probes is 'multifaceted'. In fact, two distinct research objectives can be defined. One: the unique properties and behavior of a 1D material should be exploited by its assembly into a probe in order to carry out enhanced characterization or mapping of a surface of interest. Two: the unique adhesion and friction behavior of the 1D material itself, and its intrinsic surface properties, are of primary interest, and should be fundamentally characterized. Regardless of which two objectives are sought, the experimental requirements are similar. Due to the sheer variety of recently synthesized 1D materials, and the lack of experimental data on their properties, the majority of literature has focused on their fundamental characterization over their exploitation.

The first assembled mechanical probes to exploit integrated 1D material as function elements consisted of conventional Si microcantilevers with tips decorated by a singular CNT. To improve the topographic imaging capability of AFM, the CNT was cantilevered from the existed etched tip, orientated perpendicular to the main cantilever beam, replacing the tip as the sensing element as shown in Figure 6A (Akita et al., 2000; Chen et al., 2004; Dietzel et al., 2005; Strus et al., 2005). An SEM micrograph of a CNT deposited on the sidewall of a Si tip is presented in Figure 6B. The high aspect ratio of the CNT permitted its free end to reach deep into surface pits or troughs on a textured substrate, as well as to map highly inclined side-walls. The high compliance of the CNT also avoided the transfer of large forces between tip and sample during scanning, and hence prevented tip wear or damage to delicate samples. In this way, the CNTs acted as the sensing element, with the main microcantilever beam continuing to function as the deflection element, read-out *via* the optical beam deflection approach.

CNT-microcantilever probe designs were also developed in order to fundamentally investigate the adhesive and friction behavior of the integrated CNT, and the properties of interfaces formed between a CNT and other surfaces within an air environment (Bhushan et al., 2008a; Bhushan et al., 2008b; Bhushan and Ling, 2008). One of the more successful probe designs involved fastening the CNT to a tipless microcantilever with it aligned parallel to the main beam as shown in Figure 6C (Strus et al., 2008; Strus et al., 2009). With the CNT orientated in this way, it could be attached and detached by peeling from a surface of interest in a controlled manner in order to measure adhesive forces. This technique is commonly referred to as peeling force spectroscopy (Buchoux et al., 2011; Li et al., 2015). Here, to quantify force, the deflection of the CNT was again not directly read-out, but rather deduced from the force-distance relationship obtain from the microcantilever deflection in combination with analytical or numerical mechanical deflection models.

OBDA-based microcantilever read-out strategies were employed in the above techniques as the direct read-out of 1D structures with cross-sections as small as that of an individual CNT calls for more sophisticated and expensive experimental setups. Direct read-out of a CNT's deflection profile was successfully conducted by Chen et al. in 2003, and later by Ke et al. in 2010 using the sub-atomic spatial resolution of a transmission electron microscope (TEM) as illustrated by the TEM micrographs in Figures 6D,E (Chen et al., 2003; Ke et al., 2010a). SEM imaging was later used to detect the profiles of singular CNTs (Ishikawa et al., 2008, 2009). The relatively lower resolution of SEM generally prevents the deflection profiles of smaller diameter CNTs from being resolved. Roenbeck et al., Sui et al., and Chen et al. perhaps demonstrate the lower limit in the diameters that can be resolved; reading out the deflection of CNTs with diameters of ~ 30, ~ 60, and ~ 45 nm, respectively (Roenbeck et al., 2014; Chen et al., 2016; Sui et al., 2016). In each study, the CNT profile was used to quantify their peeling force and/or surface energy, respectively. The *in-situ* SEM setup and peeling configurations employed by Chen et al. are presented in Figures 6F,G, respectively. A composite SEM micrograph showing the deflection of a CNT at three stages of peeling is

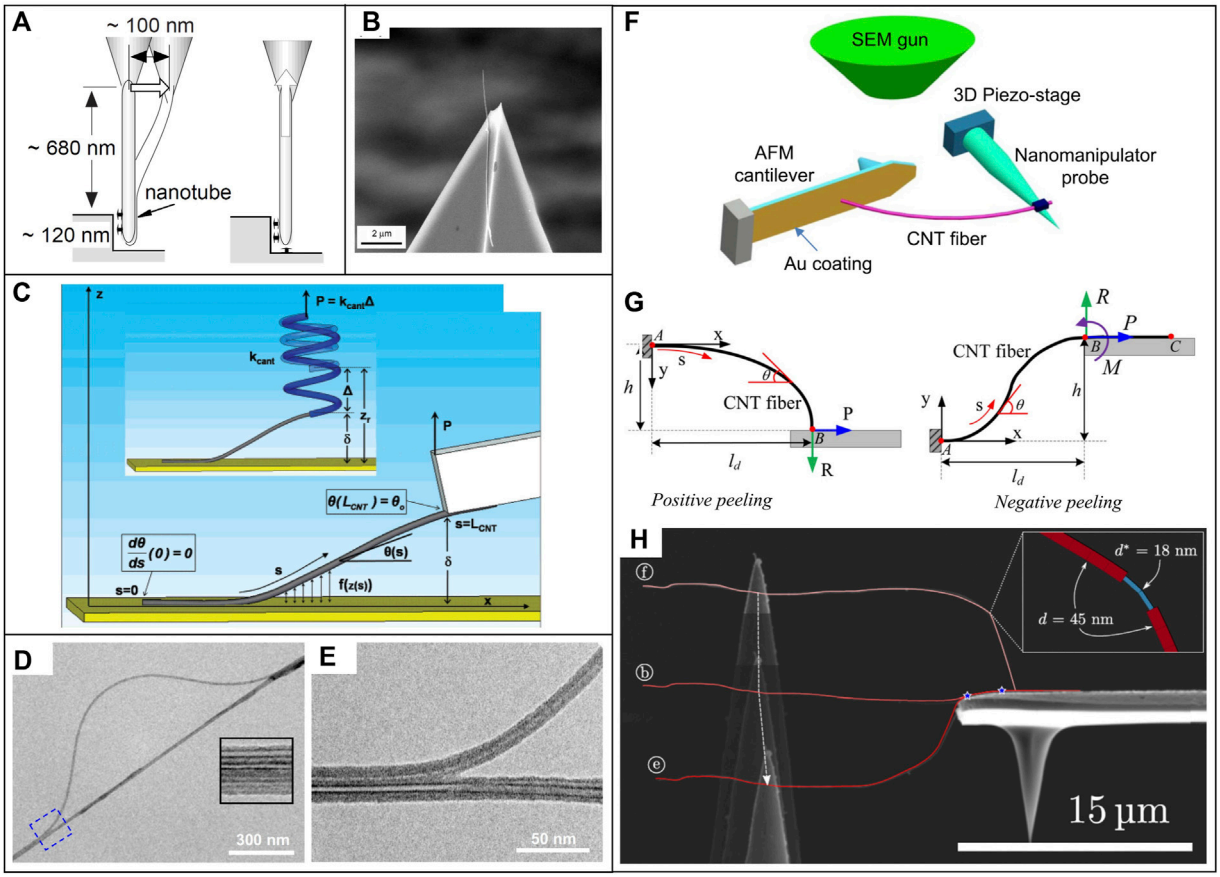

FIGURE 6
(A) Diagram of microcantilever tip decorated with CNT tip for enhanced surface topography scanning using AFM (Akita et al., 2000) **(B)** SEM micrograph of CNT deposited on the end of a microcantilever tip (Bhushan et al., 2008a). **(C)** Diagram of parallel-aligned CNT on tipless microcantilever for conducting peeling studies (Strus et al., 2008). **(D,E)** TEM micrograph observation of the buckled deflection shape of partially delaminated CNT bundle (Ke et al., 2010a). **(D)** Overview of buckled arch, and **(E)** high-resolution micrograph of delamination region. **(F–H)** *In situ* SEM imaging-based read-out of CNT probe (Chen et al., 2016). **(F)** Experimental setup. **(G)** Diagram of positive and negative peeling configuration. **(H)** Composite of 3x. SEM micrographs showing progression of CNT deflection shape.

shown in Figure 6H. SEM proved highly successful for imaging the deflection profiles of CNT bundles (which can have significantly larger cross-sections than singular CNTs), allowing the adhesion between CNTs within the bundles to be characterized (Ke et al., 2010b; Zheng and Ke, 2010).

3.3 Nanowire-based contact probes

The previously presented studies demonstrate the success of using NTs as sensor elements in mechanical contact probing, especially for topography mapping. The utilization of NTs as deflection elements, however, remained relatively limited due to the high spatial-resolution required by the read-out strategy. NWs, in contrast, can be synthesized with any cross-sectional size. The cross-section of a NWs can hence be carefully selected to suit the specific probe design or application. Specifically, when acting as a deflection element, the cross-sectional dimensions of a NW must be small enough to achieve the required force resolution (i.e. sufficiently compliant), whilst large enough to be detected by the employed readout strategy. NWs also have the additional benefit over NTs in that they can be synthesized with a broad range of compositions, crystal structures, and surface geometries. This enables the formation of well-defined contact areas for applications requiring precise force/energy quantification, and facilitates the fundamental characterization of interface with varied surface combinations.

Xie and Régnier quantified the total work of adhesion required to peel Si NWs from a substrate in air using a novel nanotweezer configuration, relying on ‘indirect’ OBDA-based readout of dual microcantilevers (Xie and Régnier, 2010). Desai and Haque brought a cantilevered ZnO NW (fastened by contact adhesion to a TEM grid) into point-contact with the top surface of a Si cantilever inside an SEM (Desai and Haque, 2007). The

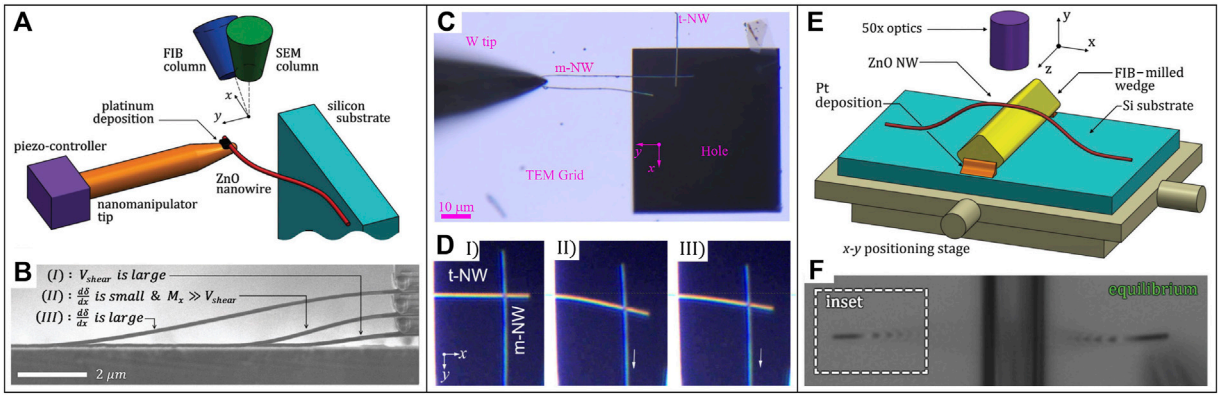

FIGURE 7
(A,B) ZnO NW peeling detection via SEM imaging-based read-out (Mead et al., 2018). **(A)** Schematic of setup. **(B)** Composite of 3x. SEM micrographs showing peeling progression of NW. **(C,D)** OM imaging-based read-out of sliding SiC NW pair (Yibibulla et al., 2022). Micrographs of **(C)** experimental configuration, and **(D)** sliding progression, at stage I, II and III. **(E,F)** OM-based interferometric read-out of partially delaminated ZnO NW arch (Mead et al., 2020). **(E)** Schematic of experiment setup. **(F)** Micrograph show visible fringe patterns on suspended segment of NW.

resulting arc-shape deflection curve was successfully read-out by SEM imaging, and used to quantify the adhesive force. *In situ* SEM-based probing was developed further by Mead et al., whereby ZnO NWs lying on a Si substrate were attached to a W tip by EBiD Pt, and peeled off in a controlled manner as shown in Figure 7A (Mead et al., 2018). The deflected s-shape of the NW during peeling shown in Figure 7B was used to obtain an adhesion energy per unit interfacial area quantity. The adhesion energy quantity, however, was an order of magnitude higher than that theoretically predicted when considering the contribution from van der Waals interactions (Israelachvili, 2011). It was deduced that electron beam irradiation and the high vacuum environment lead to modification of the interfacial and surface interactions, including the solidification of surface contaminants, EBiD carbon, and electrical charge build-up.

The enhanced adhesion energy measured by Mead et al. emphasizes that using electron microscope-based read-out strategies is typically not suitable for mechanical contact probing applications which seek to characterize adhesion behavior or surface energies. This supports further development and implementation of optics-based readout strategies beyond the commercially established OBDA towards the operation of assembled probes within ambient conditions. Numerous optical interferometric read-out strategies have been used to detect oscillating NW cantilevers (Biedermann et al., 2010). Commercially available Michelson interferometry systems have been routinely applied to NW resonance detection for elastic modulus characterization (Wang et al., 2021; Ma et al., 2022). Polarization-enhanced Michelson interferometry has been shown to obtain sufficient reflected light from NWs with diameters down to 44 nm (Nichol et al., 2008). Fabry-Perot interferometry has been used to monitor the frequency shift and direction of oscillation of a GaAs NW in 'non-contact' vectorial scanning force microscopy (Rossi et al., 2017; Braakman et al., 2018). Interferometric read-out can be conducted in air. Yet, as the majority of techniques focused on maximizing force sensitivity, the NW deflection elements were typically placed under vacuum in order to enhance their oscillation amplitude (atmospheric molecules damp oscillations). Whilst interferometric read-out has not yet been applied to NW deflection elements undergoing 'contact' probing in air, it remains a promising potential strategy.

Whilst the cross-sectional dimensions of NWs are below the diffraction-limited resolution of OM, the detection of sufficiently long NWs above a minimum diameter has been demonstrated (Ma et al., 2022). This capability has facilitated the mechanical characterization of NWs using relatively low-cost OM imaging-based read-out strategies. The arc-shape of NWs sliding along a substrate has been used to quantify their static and dynamic friction (Xie et al., 2017; Xie et al., 2018b). The loop diameter of fractured NWs have been used to quantify their fracture strength (Wang et al., 2015; Roy et al., 2017).

OM-based read-out of NWs used as contact probes has also been used to investigate their adhesion and friction behavior, as well as their surface properties. Manoharan and Haque detected snap-in of a ZnO NW probe onto a Si substrate as a sudden defocusing of its profile under an OM (Manoharan and Haque, 2009). Specifically, snap-in resulted in the NW deflected out of the optics plane, and the instance of defocusing was used as a marker to help interpret force data aquired separately from a integrated MEMS sensor. Xie et al. brought the free-ends of two perpendicular-aligned cantilevered Al_20_3 NWs into sliding contact using a W tip in order to quantify the pair's static and kinetic friction (Xie et al., 2018a). A similar configuration was used by Yibibulla et al. as shown in Figure 7C to study the

static and kinetic friction of SiC contact pairs in an environment with varying relative humidity (Yibibulla et al., 2022). Deflection of the NW contact pairs during various stages of sliding is presented in Figure 7D. Mead et al. drapped ZnO NWs over a wedge structure so that they formed arch-shaped deflection profiles whilst remaining partially adhered to the underlying Si substrate as shown in Figure 7E (Mead et al., 2020). OM-based imaging of the fringe patterns exhibited along the suspended segment of a NW, as shown in Figure 7F, were used to read-out its deflection shape and subsequently compute an adhesion energy per unit interfacial area quantity. The evaluated adhesion energy was significantly lower than that previously determined via the *in situ* SEM probing technique (Mead et al., 2018), and in line with previously experimental works where van der Waals, capillary, and electrostatic interactions contributed (Galan and Sodano, 2013). The finding of the technique was therefore considered to better reflect the adhesion behavior of NWs integrated into MEMS device that operates in ambient conditions. A downside of the static evaluation approach used in the OM-based method is that only a single location along the interface was probed. Consequently, the uncertainty associated with the evaluated adhesion energy was much higher in comparison to techniques that used a peeling configuration to probe along the length of the interface of interest.

The above works highlight that mechanical contact probes with integrated NW deflection elements which rely on OM imaging-based readout represent a powerful design pathway. OM imaging permits the probe to be operated in an ambient environment, as facilitates interface and surface characterization under different environmental conditions, including over a varying temperature and relative humidity.

4 Liquid metal probes

Considering that liquid metals offer advantageous properties such as high electrical and thermal conductivity, low vapor pressure and a hard-soft-hard interface for non-destructive measurements, the application of this material for probes is quite logical. It was at first introduced as a measuring electrode for voltammetry (Müller and Petras, 1938; Lingane and Kolthoff, 1939; Kemula et al., 1958). Applying a soft interface comes in addition to non-destructive contacting with characteristics like self-healing properties and low abrasion effects (Surmann and Zeyat, 2005; Channaa, 2008). By the introduction of gallium based liquid metals further advantages appear like high thermal and electrical conductivity, a low melting point, nearly no vapor pressure, and no toxicity (Geratherm Medical, 2004; Liu et al., 2009). The liquid phase of this material at ambient conditions allows the manipulation and structuring of desired volumes in a highly controlled manner down to the nanometer range. No complex lithographic processes are required for structuring; instead, this material can be applied to surfaces using an inkjet printer, for example (Tabatabai et al., 2013). There is a wide range of techniques that allow the manipulation of this material down to the mid-micrometer range in a top-down process. For a good insight in these techniques there are already some extensive reviews on this topic (Khondoker and Sameoto, 2016; Zuo et al., 2020). However, when targeted manipulation in the nanometer range becomes necessary, these techniques are limited to only a few that use the bottom-up method. Especially, for probe designs top-down techniques are very limited to using syringe systems (Sobczak et al., 2010) or simply by dipping a manipulator in a liquid metal reservoir (Tang et al., 2017). But going down to the submicron range, all these top-down techniques are no longer applicable, because of capillary forces and surface energies preventing these procedures. The following chapter will describe efficient bottom-up techniques for the fabrication of liquid metal probers and their application for nanoscale characterization procedures.

4.1 Fabrication techniques

For the bottom-up approach of the fabrication of liquid metal probes the liquid metal needs to be portioned in distinct volumes, deposited on dedicated spots, and further structured for functionalization. For portioning the liquid metal in volumes with diameters in the small micrometer or even nanometer range two techniques are mainly used in state-of-the-art. In the first technique a large volume of liquid metal is deposited in an acidic (e.g. HCl) solution to get rid of the oxide layer and afterwards divided into smaller volumes using a conventional blender (see Figure 8A). The size of the resulting drops can be adjusted via the speed of rotation of the blender. This emulsion is then placed on a substrate and dried. After removal of the HCl on the surface, the liquid metal droplets remain and can be further processed.

The second technique uses electromigration as a driving force for a controlled mass flow of liquid metal (see Figure 8B). Thus, liquid metal agglomerations in the nanometer range can be produced and manipulated. To start the mass flow an electrical potential between a manipulator and a liquid metal reservoir on top of a conductive substrate is applied. The manipulator (e.g. an etched tungsten wire) is negatively biased and physically connected to the reservoir. After switching on the electrical power, the liquid metal starts to flow to the cathode (p-type liquid metal; for n-type opposite direction) and material accumulates at the point where the diameter of the manipulator increases erratically. However, this is due to the fact that the driving force of electromigration strongly depends on the electric current density and decreases indirectly proportional to it when the area traversed by the current increases. Due to this abrupt decrease of the driving force, an agglomeration of material then takes place at this point. A variation of this technique is that the reservoir can also be attached to the manipulator. This allows

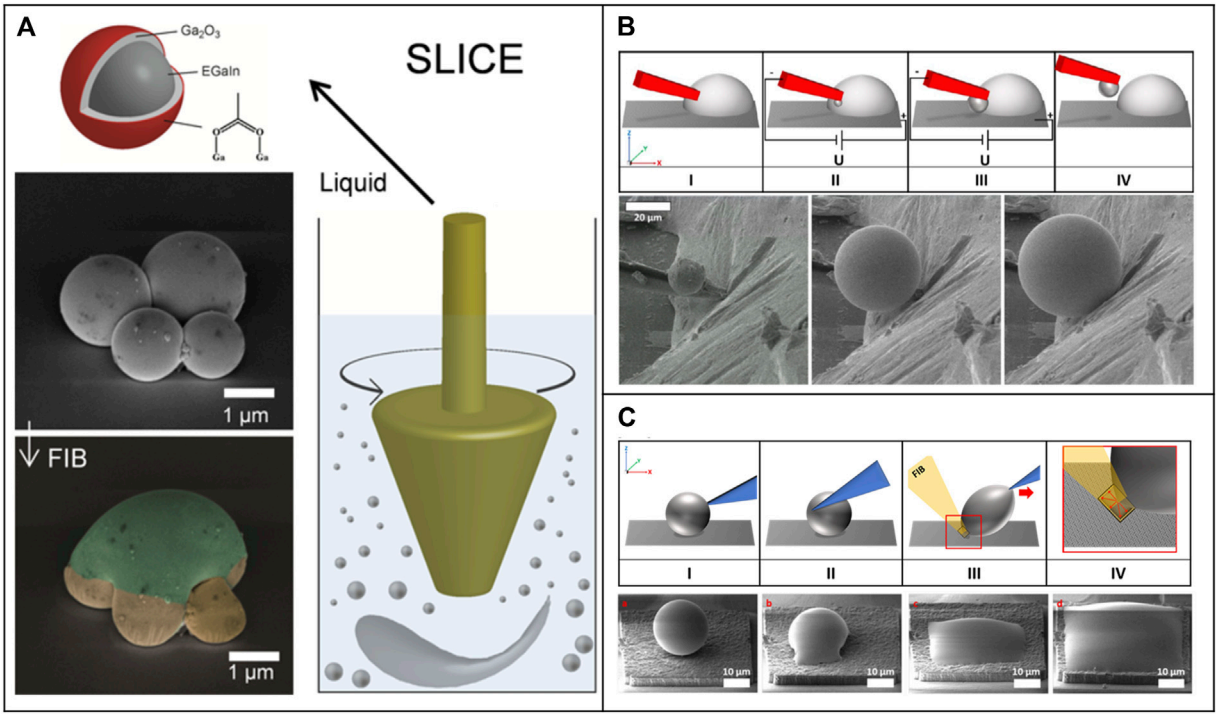

FIGURE 8
Three main techniques for manipulation of liquid metals on the small scale; **(A)** The Shearing Liquids Into Complex Particles (SLICE) Technique uses a blender for surface tension driven phase segregation. The resulting liquid metal volumes can then be merged with an FIB. Adapted with permission from (Tevis et al., 2014). Copyright 2022 American Chemical Society; **(B)** Electromigration induced mass flow can be applied for the controlled fabrication of liquid metal droplets. The mass flow strength and direction can be controlled by an external electric field. Adapted with permission from (Kleist-Retzow von et al., 2019b); **(C)** Forced wetting by ion implantation leads to the ability to structure the liquid metal to arbitrary two dimensional geometries on a defined surface. For the ion implantation an FIB system can be used. Adapted with permission from (Kleist-Retzow and von, 2021).

direct deposition of liquid metal volumes on a surface by inverting the voltage and thus positively charging the manipulator (Kleist-Retzow von et al., 2019b).

The Shearing Liquids Into Complex Particles (SLICE) technique (see Figure 8A) can produce several small volumes in parallel but has a low controllability of the diameter of the droplets in the nanometer range (Tevis et al., 2014). The fabrication of a dedicated volume with a fixed defined diameter (with nanometer precision) is a matter of luck and time. On the other side the technique using electromigration can produce one droplet with a highly controllable size in the nanometer range but has a very low throughput in the production rate. Only one sphere after another can be produced and afterwards needs to be placed on the substrate. Thus, both techniques have their advantages and disadvantages and should be selected depending on the application.

After successful portioning of the liquid into defined droplets, on the one hand the droplet itself (without further structuring) can be used for the preparation of probers. For this purpose, the forces dominating on the micrometer scale can be employed. This allows the liquid metal to be forced to adhere to a manipulator. Forces utilized for this are van-der-Waals (Guo et al., 2020), capillary (Cumby et al., 2012) and electrostatic forces (Kleist-Retzow von et al., 2019b). However, the use of these techniques makes targeted wetting or structuring of the liquid metal virtually impossible. In addition, when a substrate is contacted with a prober produced in this way, the liquid metal may remain on the contacted substrate because the adhesive forces prevail there. On the other hand, targeted wetting and structuring thus leads to a higher quality of a liquid metal probe.

For the next step, structuring the liquid metal, it must be forced to wet at certain locations, and only one technique is applicable for this on the nanometer scale. By forced wetting through ion implantation deposited liquid metal droplets can be forced to wet the contacted area (see Figure 8C) (Kleist-Retzow and von, 2021). Wetting by the liquid metal reservoir occurs during irradiation with ions in an adjacent region next to the reservoir. In this case, gallium ions (FIB) are used to induce wetting of a substrate (e.g. gold, copper, silicon) with gallium-based liquid metal. Furthermore, the

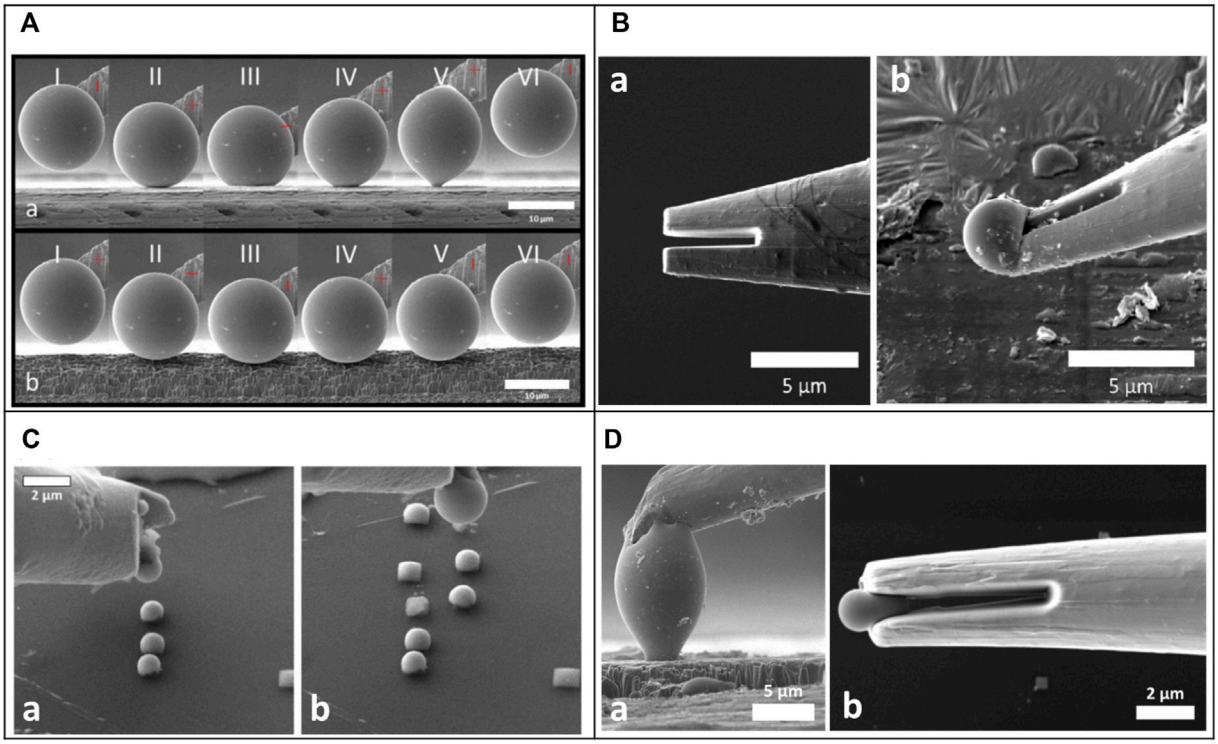

FIGURE 9
SEM micrographs of different liquid metal probers for contact applications. **(A)** Process of measuring different contact angles on a) a smooth surface and b) on a rough surface with a liquid metal (Galinstan) prober. Difference in the contact angle characteristics can be observed. Adapted with permission from (Kleist-Retzow et al., 2020); **(B)** Manipulator a) before and b) after the fabrication of a liquid metal (gallium) prober for gripping processes by phase change are illustrated. Adapted with permission from (Kleist-Retzow von et al., 2019b); **(C)** Micrographs of a liquid metal prober (Galinstan) for placing of multiple liquid metal droplets on a surface are presented. Adapted with permission from (Kleist-Retzow von et al., 2019b); **(D)** SEM micrographs of two different liquid metal probers (Galinstan) for a) contact angle measurements and b) pick and place processes are presented. Adapted with permission from (Kleist-Retzow and von, 2021).

wetting can be applied in a highly controlled manner and arbitrary two-dimensional structures can be fabricated. This technique is also applicable to increase the adhesion between a liquid metal volume and a manipulator to fabricate liquid metal probes for contact measurement procedures.

4.2 Probe design and application

The application of the versatile characteristics of liquid metals for probes comes with the ability to perform contact measurement procedures with greatly decreased abrasion and destructive effects. This advantage is especially useful for small contact areas where the influence of abrasion or surface effects have a great impact on the measurement quality. But the fabrication of liquid metal probes with contact areas in the nanometer regime can only be done by bottom-up manufacturing techniques as described before and needs highly specialized equipment and techniques.

When producing a liquid metal prober, the subsequent intended use must be considered. For example, one can attach the liquid metal as a sphere to a manipulator (see Figure 9A) or cover entire parts of the manipulator with liquid metal (see Figure 9B b) The latter variant allows better and more targeted wetting of the manipulator, which is advantageous for e.g. measurements where high contact areas are favorable, and the first variant allows e.g. contact angle measurements (see Figures 9A,D a) for which a liquid metal sphere that is as unaffected as possible is required. This implementation resulted in successful applications such as probes for contact angle measurements (Kleist-Retzow et al., 2020; Klauser et al., 2022), probes for gripping processes with adjustable adhesion (Kleist-Retzow von et al., 2019b) or probes for printing liquid metal volumes (see Figure 9C) (Kleist-Retzow von et al., 2019b).

When measuring contact angles in the nanometer range, the use of gallium-based liquid metals (such as Galinstan (Geratherm Medical, 2004)) is of great advantage because of its property of hardly measurable vapor pressure. Conventional measurement methods based on e.g. water droplets can only be used to a very

limited extent due to rapid evaporation and offer hardly any possibilities to keep the volume of the sphere constant. With the use of liquid metal, this measurement method made it possible for the first time to experimentally determine the effect of the line tension and to determine contact angles in the nanometer range (Klauser et al., 2022).

Manipulators to perform liquid metal based gripping procedures are mainly based on phase changing mechanisms. By cooling the liquid metal under the melting point the adhesion of the liquid metal increases and objects can be picked up (Ye et al., 2016; Kleist-Retzow von et al., 2019b). When the material is subsequently heated over the melting temperature, the adhesion can be reduced again, which can be used to deposit an object. This method can be used to reversibly control the adhesion between a manipulator and an object.

The major disadvantage of gallium based liquid metal, namely the oxide layer, has a major influence on all applications and plays a decisive role in the individual procedures. Despite the fact that the layer is only a few nanometers thick (Regan et al., 1997), it changes the properties of a liquid metal droplet enormously by altering the physical properties such as viscosity (Scharmann et al., 2004), conductivity (Kleist-Retzow and von, 2021) and adhesion (Ye et al., 2016; Kleist-Retzow von et al., 2019b). The formation of an oxide layer can only be prevented in a completely oxygen-free space. In reality, however, this is almost not the case. Even in a high vacuum atmosphere, parts of oxygen are still present and lead to the formation of an oxide layer in less than an hour (Kleist-Retzow et al., 2020). However, subsequent removal is possible, for example, by using an FIB (Tevis et al., 2014; Kleist-Retzow and von, 2021).

The manipulator itself also plays an important role for liquid metal probes. By selecting an optimized geometrical design, the position of the liquid metal on the manipulator can be influenced. Since the probes presented were largely produced by electromigration, the deposition location of the liquid metal droplet can be controlled via a pre-defined shape of the manipulator. Here, the two-prong design has proven to be very effective (see Figure 9B a). On the one hand, this allows the droplet generation point and the droplet diameter to be highly controllable, and on the other hand, a high contact area between the droplet and the manipulator can be realized. A large contact area is very important for the adhesion between the droplet and the manipulator. Otherwise, if the liquid metal comes into contact with a measuring surface, the liquid metal does stick to the surface and tears off from the manipulator.

5 Perspective and future outlook

The three different types assembled mechanical probes highlighted in this review help to clarify what improved functionality can be achieved over conventional top-down fabricated probes. Their respective characteristics regarding dimensions, materials, advantages, and disadvantages are summarized in Table 2. Nevertheless, the small-scale characterization and mapping of surfaces in both physical and biological sciences can be further advanced by deeper investigation into each probe type.

The future development and application of colloidal particle probes with high-aspect ratios could benefit from improved automation of assembly processes, further miniaturization of the employed particles, as well as further diversification of the particle materials. The implementation of an automation approach can increase the throughput and repeatability of the measurements. However, to realize a fully automated assembly, calibration, and measurement procedure would require significant engineering efforts as well as tackling problems such as electron beam induced drift and parasitic EBiD as the process takes place inside the SEM. Furthermore, the implementation of particles smaller than 500 nm in diameter requires further development of reliable handling approaches and feedback systems and automation algorithms but would allow to investigate nanoscale adhesion and friction phenomena even further. Moreover, additive manufacturing techniques such as sintering and EBiD have been employed to fabricate e.g. alumina and zirconia microparticles as mentioned in section 2.1 and used for tip modification (Sqalli et al., 2002), respectively. Further development of additive manufacturing techniques has the potential to contribute to a larger variety of materials and faster and easier probe fabrication, if challenges regarding repeatability, uniform geometry, low surface roughness are overcome and contaminations can be avoided.

Furthermore, the potential for probes based on colloidal particles to reveal more about the friction and adhesion properties of 2D materials, as well as the degradation of nanoplastics and biological samples has only been uncovered and leaves plenty of room for future research. Additionally, high aspect ratio colloidal probes could significantly contribute to understanding the influence of the electron beam on nanoscale adhesion inside the SEM where the influence of the cantilever beam and possible contaminations could not be excluded by previous probe designs (Zimmermann and Huang, 2019).

Mechanical contact probes that utilize NWs as the deflection element stand to benefit from the further development OM imaging-based read-out strategies. Current literature in Chapter 3 had shown that OM imaging is an ideal read-out strategy as it permits probes to operate in an ambient environment and is able to detect NWs with relatively small diameters. Current literature had also shown that the s-shaped NW peeling configuration was effective for characterizing surfaces and interfacial properties (Strus et al., 2008; Mead et al., 2018), and yet such a configuration has not been implemented in the OM environment. Implementation of the

TABLE 2 Summary of characteristics of the bottom up fabricated contact probe designs discussed in this work.

Technique	Material	Dimensions	Advantages	Disadvantages
1D probes	carbon nanotubes (CNT) Akita et al. (2000); Chen et al. (2003); Bhushan et al. (2008a); Bhushan et al. (2008b); Ishikawa et al. (2008); Strus et al. (2008); Strus et al. (2009); Buchoux et al. (2011); Roenbeck et al. (2014); Li et al. (2015)	Cross-section: single-walled to multi-walled. Diameter: 1.43–75 nm	When 1D material is used as deflection element: • High compliance facilitates high force sensitivity • Precise geometry facilitates accurate mechanical modelling	When 1D material is used as deflection element: • Complex ad unstable buckling behaviour during contact with sample • Diameter too small for conventional read-out strategies (i.e. optical beam deflection approach) • Single-location deflection read-out is insufficient. Read-out of entire deflection shape is required • Highly distorted shape typically requires complex analytical or numerical models
	boron nitride nanotubes Zhao et al. (2014)	Cross-section: double-walled. Diameter: 2.21–4.67 nm	When 1D material is used as sensor element: • Large variety of material compositions allows study of various interface chemistries • Crystal structures with low defect densities and well-defined surface termination provides predictable interfacial interactions	When 1D material is used as deflection element: • Probe-sample contact area occurs as line-contact, which is typically complex to quantify
	CNT fibres/bundles (of single-walled CNT) Ke et al. (2010a); Ke et al. (2010b); Zheng and Ke, (2010); Chen et al. (2016)	Cross-section: lateral width: 13.4–45 nm		
	ZnO nanowires Desai and Haque, (2007); Manoharan and Haque, (2009); Mead et al. (2018); Mead et al. (2020)	Cross-section: hexagonal. Effective diameter: ≈ 100–300 nm		
	Si nanowires Xie and Régnier, (2010)	Cross-section: highly tapered along length		
	SiC nanowires Yibibulla et al. (2022)	Cross-section: irregular/ hexagonal. Facet length: 93–120 nm		
	Al_20_3 nanowires Xie et al. (2018a)	Cross-section: rectangular cross-section. width: 298–697 nm height: 150–280 nm		
Liquid metal probes	Galinstan Kleist-Retzow et al. (2019b), EGaIn Tevis et al. (2014), Ga Kleist-Retzow et al. (2019a)	50 nm up to several mm (depends on technique)	High electrical and thermal conductivity, soft material, restructurable, self-healing	Oxide layer changes characteristics (e.g. viscosity, conductivity), chemical reacting (e.g. with O_2, Au, Al)
Colloidal particle probes	Si Ducker et al. (1991), ZnS Gillies et al. (2005), Al_2O_3 Nalaskowski et al. (2003), glass Butt, (1991); Kokkoli and Zukoski, (2000), zirconia Pedersen and Bergström, (1999), TiO_2 Larson et al. (1993), MgO Kauppi et al. (2005), PS, PMMA, MF Zimmermann et al. (2020), irregular particles/single crystals Finot et al. (1999), potentially also environmental particles	Few 10s of nm to mm-range	Known geometry (except for environmental/irregular particles), comparably easy adhesion energy calculation, a variety of materials and sphere sizes available	Possible contamination during assembly process, limited material choice for each specific assembly technique

peeling configuration in combination with OM could overcome the challenges that are presented by *in situ* SEM probing (Mead et al., 2018), and yet also reduce the uncertainty associated with the existing OM-based static test (Mead et al., 2020). The additional advantage of OM image-based read-out as highlighted in Chapter 3, is that it facilitates probe operation

in a range of environments, including over a range of temperatures and relative humidity. The systematic operation of NW-based mechanical probes over a range of environmental conditions could provide valuable data on how NWs behave within a MEMS device. In addition, only a select number of NW compositions have been exploited in the assembly of mechanical probes, leaving the surface properties of a vast number of NW compositions yet to be experimentally characterized. On a separate note, Chapter 3 also emphasized that interferometric read-out strategies have only been applied to NWs in the non-contact regime. Proof-of-concept investigation of whether interferometric read-out can be applied to detecting NWs whilst in partial contact may yield interesting results. Finally, as with many assembled probe designs, the use of serial pick-and-place strategies certainly introduces a high cost-barrier to their wide-spread use by the scientific community. Therefore, the significant challenge of developing effective parallel assembly methods must continue to be explored.

The application of liquid metal probers for adhesion measurements has been described in the literature in the last years. However, this field of research still offers numerous possibilities for optimization and modification. One of these possibilities would be a complete automation of the entire process flow. This includes the production of a new droplet, the functionalization of a probe with the droplet and the subsequent contact measurements. Furthermore, this method offers the unique possibility to utilize and simultaneously connect different measurement principles within the same probe design. Thus, state-of-the-art measurement methods such as contact angle measurements can be expanded to the nanometer range, providing new information on interface and surface effects. Furthermore, the possibility of specifically changing the adhesive forces of the liquid metal via the phase change and using it as a gripper also offers great development potential. More precise control of the targeted temperature change should be addressed through further research and the process should be fully automated. The great advantage of this method is the advanced form-fitting process, which results in little interference with the gripped object. Additionally, it would be valuable to investigate ways to provide an oxide-free liquid metal that can be applied to the probe, or to design a contact surface that would reduce the oxide layer on the probe.

Author contributions

JM, WK, FvK-R: contributed equally to this work, including conceptualization, writing, reviewing, and editing. (WK: Chapter 2. JM: Chapter 3. FvK-R: Chapter 4.) SF: Conceptualization and supervision.

Funding

This work was supported by the German Research Foundation (DFG), grant number GZ: FA347/54-1 (LiCoPro) and grant number GZ: FA 347/55-1 (UlSuFo), and the Federal Ministry of Education and Research (BMBF) under grant number 13GW0402B (ForMat-Cardio).

Conflict of interest

The authors declare that the research was conducted in the absence of any commercial or financial relationships that could be construed as a potential conflict of interest.

Publisher's note

All claims expressed in this article are solely those of the authors and do not necessarily represent those of their affiliated organizations, or those of the publisher, the editors and the reviewers. Any product that may be evaluated in this article, or claim that may be made by its manufacturer, is not guaranteed or endorsed by the publisher.

References

Akita, S., Nishijima, H., Kishida, T., and Nakayama, Y. (2000). Influence of force acting on side face of carbon nanotube in atomic force microscopy. *J. Appl. Phys.* 39, 3724–3727. doi:10.1143/jjap.39.3724

Albrecht, T. R., Akamine, S., Carver, T. E., and Quate, C. F. (1990). Microfabrication of cantilever styli for the atomic force microscope. *J. Vac. Sci. Technol. A Vac. Surfaces Films* 8, 3386–3396. doi:10.1116/1.576520

Anselme, K., Ploux, L., and Ponche, A. (2010). Cell/material interfaces: Influence of surface chemistry and surface topography on cell adhesion. *J. Adhesion Sci. Technol.* 24, 831–852. doi:10.1163/016942409X12598231568186

Arash, B., Wang, Q., and Varadan, V. K. (2014). Mechanical properties of carbon nanotube/polymer composites. *Sci. Rep.* 4, 6479. doi:10.1038/srep06479

Archard, J. E. (1957). Elastic deformation and the laws of friction. Proceedings of the royal society of London. *Series A. Mathematical physical sci.* 243, 190–205. doi:10.1098/rspa.1957.0214

Babcock, K., Elings, V., Dugas, M., and Loper, S. (1994). Optimization of thin-film tips for magnetic force microscopy. *IEEE Trans. Magn.* 30, 4503–4505. doi:10.1109/20.334130

Benz, M., Rosenberg, K. J., Kramer, E. J., and Israelachvili, J. N. (2006). The deformation and adhesion of randomly rough and patterned surfaces. *J. Phys. Chem.* B110, 11884–11893. doi:10.1021/jp0602880

Bhushan, B., and Ling, X. (2008). Adhesion and friction between individual carbon nanotubes measured using force-versus-distance curves in atomic force microscopy. *Phys. Rev. B* 78, 045429. doi:10.1103/physrevb.78.045429

Bhushan, B., Galasso, B., Bignardi, C., Nguyen, C. V., Dai, L., and Qu, L. (2008a). Adhesion, friction and wear on the nanoscale of MWNT tips and SWNT and MWNT arrays. *Nanotechnology* 19, 125702. doi:10.1088/0957-4484/19/12/125702

Bhushan, B., Ling, X., Jungen, A., and Hierold, C. (2008b). Adhesion and friction of a multiwalled carbon nanotube sliding against single-walled carbon nanotube. *Phys. Rev. B* 77, 165428. doi:10.1103/PhysRevB.77.165428

Bhushan, B. (2005). Nanotribology and nanomechanics. *Wear* 259, 1507–1531. doi:10.1016/j.wear.2005.01.010

Biedermann, L. B., Tung, R. C., Raman, A., Reifenberger, R. G., Yazdanpanah, M. M., and Cohn, R. W. (2010). Characterization of silver–gallium nanowires for force and mass sensing applications. *Nanotechnology* 21, 305701. doi:10.1088/0957-4484/21/30/305701

Binnig, Q., and Gerber, C. (1986). Atomic force microscope. *Phys. Rev. Lett.* 56, 930–933. doi:10.1103/PhysRevLett.56.930

Bohidar, H. B., and Rawat, K. (2017). *Design of nanostructures: Self-assembly of nanomaterials*. Hoboken, NJ, United States: John Wiley & Sons.

Bonaccurso, E., Kappl, M., and Butt, H.-J. (2002). Hydrodynamic force measurements: Boundary slip of water on hydrophilic surfaces and electrokinetic effects. *Phys. Rev. Lett.* 88, 076103. doi:10.1103/PhysRevLett.88.076103

Braakman, F. R., Rossi, N., Tütüncüoglu, G., Morral, A. F. i., and Poggio, M. (2018). Coherent two-mode dynamics of a nanowire force sensor. *Phys. Rev. Appl.* 9, 054045. doi:10.1103/PhysRevApplied.9.054045

Braithwaite, G. J. C., Howe, A., and Luckham, P. F. (1996). Interactions between poly(ethylene oxide) layers adsorbed to glass surfaces probed by using a modified atomic force microscope. *Langmuir* 12, 4224–4237. doi:10.1021/la960154l

Brissinger, D., Parent, G., and Lacroix, D. (2013). Note: Mechanical etching of atomic force microscope tip and microsphere attachment for thermal radiation scattering enhancement. *Rev. Sci. Instrum.* 84, 126106. doi:10.1063/1.4849575

Buchoux, J., Bellon, L., Marsaudon, S., and Aimé, J.-P. (2011). Carbon nanotubes adhesion and nanomechanical behavior from peeling force spectroscopy. *Eur. Phys. J. B* 84, 69–77. doi:10.1140/epjb/e2011-20204-1

Butt, H.-J., Cappella, B., and Kappl, M. (2005). Force measurements with the atomic force microscope: Technique, interpretation and applications. *Surf. Sci. Rep.* 59, 1–152. doi:10.1016/j.surfrep.2005.08.003

Butt, H.-J. (1991). Measuring electrostatic, van der Waals, and hydration forces in electrolyte solutions with an atomic force microscope. *Biophysical J.* 60, 1438–1444. doi:10.1016/S0006-3495(91)82180-4

Cannara, R. J., Eglin, M., and Carpick, R. W. (2006). Lateral force calibration in atomic force microscopy: A new lateral force calibration method and general guidelines for optimization. *Rev. Sci. Instrum.* 77, 053701. doi:10.1063/1.2198768

Cao, G., and Liu, D. (2008). Template-based synthesis of nanorod, nanowire, and nanotube arrays. *Adv. Colloid Interface Sci.* 136, 45–64. doi:10.1016/j.cis.2007.07.003

Channaa, H. (2008). *Eine neuartige Metallelektrode als Alternative zur Quecksilberelektrode*. Doctoral dissertation. Berlin, Germany: Freie Universität Berlin. Available at: https://refubium.fu-berlin.de/bitstream/handle/fub188/13746/DissChannaa.pdf?sequence=1.

Chen, B., Gao, M., Zuo, J. M., Qu, S., Liu, B., and Huang, Y. (2003). Binding energy of parallel carbon nanotubes. *Appl. Phys. Lett.* 83, 3570–3571. doi:10.1063/1.1623013

Chen, L., Cheung, C. L., Ashby, P. D., and Lieber, C. M. (2004). Single-Walled carbon nanotube AFM probes: Optimal imaging resolution of nanoclusters and biomolecules in ambient and fluid environments. *Nano Lett.* 4, 1725–1731. doi:10.1021/nl048986o

Chen, X., Zheng, M., Wei, Q., Signetti, S., Pugno, N. M., and Ke, C. (2016). Deformation of nanotubes in peeling contact with flat substrate: An *in situ* electron microscopy nanomechanical study. *J. Appl. Phys.* 119, 154305. doi:10.1063/1.4945995

Chighizola, M., Puricelli, L., Bellon, L., and Podestà, A. (2021). Large colloidal probes for atomic force microscopy: Fabrication and calibration issues. *J. Mol. Recognit.* 34, e2879. doi:10.1002/jmr.2879

Chung, K.-H., Pratt, J. R., and Reitsma, M. G. (2010). Lateral force calibration: Accurate procedures for colloidal probe friction measurements in atomic force microscopy. *Langmuir* 26, 1386–1394. doi:10.1021/la902488r

Cleland, A. N., and Roukes, M. L. (2002). Noise processes in nanomechanical resonators. *J. Appl. Phys.* 92, 2758–2769. doi:10.1063/1.1499745

Cross, S. E., Jin, Y.-S., Tondre, J., Wong, R., Rao, J., and Gimzewski, J. K. (2008). AFM-based analysis of human metastatic cancer cells. *Nanotechnology* 19, 384003. doi:10.1088/0957-4484/19/38/384003

Cumby, B. L., Hayes, G. J., Dickey, M. D., Justice, R. S., Tabor, C. E., and Heikenfeld, J. C. (2012). Reconfigurable liquid metal circuits by Laplace pressure shaping. *Appl. Phys. Lett.* 101, 174102. doi:10.1063/1.4764020

Dalvi, S., Gujrati, A., Khanal, S. R., Pastewka, L., Dhinojwala, A., and Jacobs, T. D. B. (2019). Linking energy loss in soft adhesion to surface roughness. *Proc. Natl. Acad. Sci. U. S. A.* 116, 25484–25490. doi:10.1073/pnas.1913126116

Dasgupta, N. P., Sun, J., Liu, C., Brittman, S., Andrews, S. C., Lim, J., et al. (2014). 25th anniversary article: Semiconductor nanowires – synthesis, characterization, and applications. *Adv. Mat.* 26, 2137–2184. doi:10.1002/adma.201305929

Derjaguin, B. V., Muller, V. M., and Toporov, Y. P. (1975). Effect of contact deformations on the adhesion of particles. *J. Colloid Interface Sci.* 53, 314–326. doi:10.1016/0021-9797(75)90018-1

Desai, A. V., and Haque, M. A. (2007). Sliding of zinc oxide nanowires on silicon substrate. *Appl. Phys. Lett.* 90, 033102. doi:10.1063/1.2431712

Diebold, A. V., Watson, A. M., Holcomb, S., Tabor, C., Mast, D., Dickey, M. D., et al. (2017). Electrowetting-actuated liquid metal for RF applications. *J. Micromech. Microeng.* 27, 025010. doi:10.1088/1361-6439/aa556a

Dietzel, D., Faucher, M., Iaia, A., Aimé, J. P., Marsaudon, S., Bonnot, A. M., et al. (2005). Analysis of mechanical properties of single wall carbon nanotubes fixed at a tip apex by atomic force microscopy. *Nanotechnology* 16, S73–S78. doi:10.1088/0957-4484/16/3/014

Duan, X., and Lieber, C. M. (2000). General synthesis of compound semiconductor nanowires. *Adv. Mat.* 12, 298–302. doi:10.1002/(SICI)1521-4095(200002)12:4<298:AID-ADMA298>3.0.CO;2-Y

Ducker, W. A., Senden, T. J., and Pashley, R. M. (1991). Direct measurement of colloidal forces using an atomic force microscope. *Nature* 353, 239–241. doi:10.1038/353239a0

Dukic, M., Adams, J. D., and Fantner, G. E. (2015). Piezoresistive AFM cantilevers surpassing standard optical beam deflection in low noise topography imaging. *Sci. Rep.* 5, 16393. doi:10.1038/srep16393

Finot, E., Lesniewska, E., Mutin, J.-C., and Goudonnet, J.-P. (1999). Investigations of surface forces between gypsum crystals in electrolytic solutions using microcantilevers. *J. Chem. Phys.* 111, 6590–6598. doi:10.1063/1.479950

Fischer, K. E., Alemán, B. J., Tao, S. L., Daniels, R. H., Li, E. M., Bünger, M. D., et al. (2009). Biomimetic nanowire coatings for next generation adhesive drug delivery systems. *Nano Lett.* 9, 716–720. doi:10.1021/nl803219f

Fischer-Cripps, A. C. (2000). *Introduction to contact mechanics*. New York, NY, USA: Springer.

Fuller, K. N. G., and Tabor, D. (1975). The effect of surface roughness on the adhesion of elastic solids. *Proc. R. Soc. Lond.* A345, 327–342. doi:10.1098/rspa.1975.0138

Galan, U., and Sodano, H. A. (2013). Intermolecular interactions dictating adhesion between ZnO and graphite. *Carbon* 63, 517–522. doi:10.1016/j.carbon.2013.07.027

Gan, Y. (2005). Attaching spheres to cantilevers for colloidal probe force measurements: A simplified technique. *Micros. Today* 13, 48–50. doi:10.1017/S155192950005402X

Garnett, E., Mai, L., and Yang, P. (2019). Introduction: 1D nanomaterials/nanowires. *Chem. Rev.* 119, 8955–8957. doi:10.1021/acs.chemrev.9b00423

Geratherm Medical, A. G. (2004). *Galinstan fluid-safety data sheet acc, to guideline 93/112/EC*. Tampa, FL, United States: Vector Solutions.

Gillies, G., Kappl, M., and Butt, H.-J. (2005). Surface and capillary forces encountered by zinc sulfide microspheres in aqueous electrolyte. *Langmuir* 21, 5882–5886. doi:10.1021/la050226l

Gong, J., Xu, B., Yang, Y., Wu, M., and Yang, B. (2020). An adhesive surface enables high-performance mechanical energy harvesting with unique frequency-insensitive and pressure-enhanced output characteristics. *Adv. Mat.* 32, 1907948. doi:10.1002/adma.201907948

Greenwood, J. A., Williamson, J. B. P., and Bowden, F. P. (1966). Contact of nominally flat surfaces. *Proc. R. Soc. Lond. Ser. A. Math. Phys. Sci.* 295, 300–319. doi:10.1098/rspa.1966.0242

Greenwood, J. A. (1997). Adhesion of elastic spheres. *Proc. R. Soc. Lond. A* 453, 1277–1297. doi:10.1098/rspa.1997.0070

Guo, J., Wang, Y., Wang, X., Xing, Y., and Hu, L. (2020). On-demand manipulation of liquid metal droplet via van der Waals adhesion. *Adv. Mat. Interfaces* 7, 2000732. doi:10.1002/admi.202000732

Helfricht, N., Mark, A., Dorwling-Carter, L., Zambelli, T., and Papastavrou, G. (2017). Extending the limits of direct force measurements: Colloidal probes from sub-micron particles. *Nanoscale* 9, 9491–9501. doi:10.1039/c7nr02226c

Hernández-Vélez, M. (2006). Nanowires and 1D arrays fabrication: An overview. *Thin Solid Films* 495, 51–63. doi:10.1016/j.tsf.2005.08.331

Holzinger, M., Le Goff, A., and Cosnier, S. (2014). Nanomaterials for biosensing applications: A review. *Front. Chem.* 2, 63. doi:10.3389/fchem.2014.00063

Hsieh, H.-H., and Wu, C.-C. (2007). Amorphous ZnO transparent thin-film transistors fabricated by fully lithographic and etching processes. *Appl. Phys. Lett.* 91, 013502. doi:10.1063/1.2753724

Indrieri, M., Podestà, A., Bongiorno, G., Marchesi, D., and Milani, P. (2011). Adhesive-free colloidal probes for nanoscale force measurements: Production and characterization. *Rev. Sci. Instrum.* 82, 023708. doi:10.1063/1.3553499

Ishikawa, M., Harada, R., Sasaki, N., and Miura, K. (2008). Visualization of nanoscale peeling of carbon nanotube on graphite. *Appl. Phys. Lett.* 93, 083122. doi:10.1063/1.2959188

Ishikawa, M., Harada, R., Sasaki, N., and Miura, K. (2009). Adhesion and peeling forces of carbon nanotubes on a substrate. *Phys. Rev. B* 80, 193406. doi:10.1103/physrevb.80.193406

Israelachvili, J. N. (2011). *Intermolecular and surface forces*. London, UK: Academic Press.

Jacobs, T. D. B., and Martini, A. (2017). Measuring and understanding contact area at the nanoscale: A review. *Appl. Mech. Rev.* 69. doi:10.1115/1.4038130

Janshoff, A., Neitzert, M., Oberdörfer, Y., and Fuchs, H. (2000). Force spectroscopy of molecular systems—single molecule spectroscopy of polymers and biomolecules. *Angew. Chem. Int. Ed.* 39, 3212–3237. doi:10.1002/1521-3773(20000915)39:18<3212:AID-ANIE3212>3.0.CO;2-X

Jia, C., Lin, Z., Huang, Y., and Duan, X. (2019). Nanowire electronics: From nanoscale to macroscale. *Chemical Rev.* 119, 9074–9135. doi:10.1021/acs.chemrev.9b00164

Jiang, Y., and Turner, K. T. (2016). Measurement of the strength and range of adhesion using atomic force microscopy. *Extreme Mech. Lett.* 9, 119–126. doi:10.1016/j.eml.2016.05.013

Johnson, K. L., Kendall, K., and Roberts, A. D. (1971). Surface energy and the contact of elastic solids. *Proc. R. Soc. Lond. A. Math. Phys. Sci.* 324, 301. doi:10.1098/rspa.1971.0141

Kappl, M., and Butt, H.-J. (2002). The colloidal probe technique and its application to adhesion force measurements. *Part. Part. Syst. Charact.* 19, 129. doi:10.1002/1521-4117(200207)19:3<129:AID-PPSC129>3.0.CO;2-G

Karaman, M. E., Meagher, L., and Pashley, R. M. (1993). Surface chemistry of emulsion polymerization. *Langmuir* 9, 1220–1227. doi:10.1021/la00029a012

Kauppi, A., Andersson, K. M., and Bergström, L. (2005). Probing the effect of superplasticizer adsorption on the surface forces using the colloidal probe AFM technique. *Cem. Concr. Res.* 35, 133–140. doi:10.1016/j.cemconres.2004.07.008

Ke, C., Zheng, M., Bae, I.-T., and Zhou, G. (2010a). Adhesion-driven buckling of single-walled carbon nanotube bundles. *J. Appl. Phys.* 107, 104305. doi:10.1063/1.3374469

Ke, C., Zheng, M., Zhou, G., Cui, W., Pugno, N., and Miles, R. N. (2010b). Mechanical peeling of free-standing single-walled carbon-nanotube bundles. *Small* 6, 438–445. doi:10.1002/smll.200901807

Kemula, W., galus, Z., and Kublik, Z. (1958). Application of the hanging mercury drop electrode to an investigation of intermetallic compounds in mercury. *Nature* 182, 1228–1229. doi:10.1038/1821228a0

Khalili, A. A., and Ahmad, M. R. (2015). A review of cell adhesion studies for biomedical and biological applications. *Intern. J. Molecular Sci.* 16, 18149–18184. doi:10.3390/ijms160818149

Khondoker, M. A. H., and Sameoto, D. (2016). Fabrication methods and applications of microstructured gallium based liquid metal alloys. *Smart Mat. Struct.* 25, 093001. doi:10.1088/0964-1726/25/9/093001

Kim, J. H., Pham, T. V., Hwang, J. H., Kim, C. S., and Kim, M. J. (2018). Boron nitride nanotubes: Synthesis and applications. *Nano Converg.* 5, 17. doi:10.1186/s40580-018-0149-y

Klauser, W., Kleist-Retzow, F., and Fatikow, S. (2022). Line tension and drop size dependence of contact angle at the nanoscale. *Nanomater. (Basel)* 12, 369. doi:10.3390/nano12030369

von Kleist-Retzow, F. T. (2021). Robotic liquid metal manipulation and electrical contact probing at small scales. doctoral dissertation. Munich, Germany: Verlag Dr. Hut GmbH. Available at: https://www.dr.hut-verlag.de/978-3-8439-4828-9.html

Kleist-Retzow, F. T., Bartenwerfer, M., and Fatikow, S. (2019a). "Liquid metal-based manipulator for microscale handling inside SEM," in 2019 IEEE 14th International Conference on Nano/Micro Engineered and Molecular Systems (NEMS) (IEEE).

Kleist-Retzow, F. T. von, Haenssler, O. C., and Fatikow, S. (2019b). Manipulation of liquid metal inside an SEM by taking advantage of electromigration. *J. Microelectromech. Syst.* 28, 88–94. doi:10.1109/JMEMS.2018.2878320

Kleist-Retzow, F., Klauser, W., Zimmermann, S., and Fatikow, S. (2020). Assessing micro- and nanoscale adhesion via liquid metal-based contact angle measurements in vacuum. *J. Mat. Sci.* 55, 4073–4080. doi:10.1007/s10853-019-04253-6

Kokkoli, E., and Zukoski, C. F. (2000). Interaction forces between hydrophobic and hydrophilic self-assembled monolayers. *J. Colloid Interface Sci.* 230, 176–180. doi:10.1006/jcis.2000.7089

Kwiat, M., Cohen, S., Pevzner, A., and Patolsky, F. (2013). Large-scale ordered 1D-nanomaterials arrays: Assembly or not? *Nano Today* 8, 677–694. doi:10.1016/j.nantod.2013.12.001

Laermer, F., Franssila, S., Sainiemi, L., and Kolari, K. (2020). "Chapter 16 - deep reactive ion etching," in *Handbook of silicon based MEMS materials and technologies. Micro and nano technologies*. Editors M. Tilli, M. Paulasto-Krockel, M. Petzold, H. Theuss, T. Motooka, and V. Lindroos. Third Edition (Elsevier), 417–446.

Larson, I., Drummond, C. J., Chan, D. Y. C., and Grieser, F. (1993). Direct force measurements between titanium dioxide surfaces. *J. Am. Chem. Soc.* 115, 11885–11890. doi:10.1021/ja00078a029

Li, T., Ayari, A., and Bellon, L. (2015). Adhesion energy of single wall carbon nanotube loops on various substrates. *J. Appl. Phys.* 117, 164309. doi:10.1063/1.4919355

Lingane, J. J., and Kolthoff, I. M. (1939). Fundamental studies with the dropping mercury electrode. I. The ilkovic equation of polarographic diffusion currents. *J. Am. Chem. Soc.* 61, 825–834. doi:10.1021/ja01873a016

Liu, X., Katehi, L. P. B., and Peroulis, D. (2009). "Non-toxic liquid metal microstrip resonators," in 2009 Asia Pacific Microwave Conference (IEEE), 131–134.

Lorenz, B., and Persson, B. N. J. (2009). Interfacial separation between elastic solids with randomly rough surfaces: comparison of experiment with theory. *Chinese Phys. Lett.* 21, 15003. doi:10.1088/0953-8984/21/1/015003

Lu, P. J., and Weitz, D. A. (2013). Colloidal particles: Crystals, glasses, and gels. *Annu. Rev. Condens. Matter Phys.* 4, 217–233. doi:10.1146/annurev-conmatphys-030212-184213

Ma, L., Yibibulla, T., Jiang, Y., Mead, J. L., Lu, M., Wang, S., et al. (2022). Temperature and size dependent mechanical properties of vapor synthesized zinc tungstate nanowires. *Phys. E Low-dimensional Syst. Nanostructures* 136, 114990. doi:10.1016/j.physe.2021.114990

Majumdar, A., and Bhushan, B. (1990). Role of fractal geometry in roughness characterization and contact mechanics of surfaces. *J. Tribology* 115, 205–216. doi:10.1115/1.2920243

Mak, L. H., Knoll, M., Weiner, D., Gorschlüter, A., Schirmeisen, A., and Fuchs, H. (2006). Reproducible attachment of micrometer sized particles to atomic force microscopy cantilevers. *Rev. Sci. Instrum.* 77, 046104. doi:10.1063/1.2190068

Manoharan, M. P., and Haque, M. A. (2009). Role of adhesion in shear strength of nanowire–substrate interfaces. *J. Phys. D. Appl. Phys.* 42, 095304. doi:10.1088/0022-3727/42/9/095304

Mark, A., Helfricht, N., Rauh, A., Karg, M., and Papastavrou, G. (2019). The next generation of colloidal probes: A universal approach for soft and ultra-small particles. *Small* 15, 1902976. doi:10.1002/smll.201902976

Maszara, W. P., Goetz, G., Caviglia, A., and McKitterick, J. B. (1988). Bonding of silicon wafers for silicon-on-insulator. *J. Appl. Phys.* 64, 4943–4950. doi:10.1063/1.342443

Maugis, D. (1992). Adhesion of spheres: The JKR-DMT transition using a dugdale model. *J. Colloid Interface Sci.* 150, 243–269. doi:10.1016/0021-9797(92)90285-T

Mead, J. L., Xie, H., Wang, S., and Huang, H. (2018). Enhanced adhesion of ZnO nanowires during *in situ* scanning electron microscope peeling. *Nanoscale* 10, 3410–3420. doi:10.1039/C7NR09423J

Mead, J. L., Wang, S., Zimmermann, S., and Huang, H. (2020). Interfacial adhesion of ZnO nanowires on a Si substrate in air. *Nanoscale* 12, 8237–8247. doi:10.1039/D0NR01261K

Megson, T. H. G. (2005). *Structural and stress analysis*. Oxford, UK: Butterworth-Heinemann.

Mielke, S. L., Troya, D., Zhang, S., Li, J.-L., Xiao, S., Car, R., et al. (2004). The role of vacancy defects and holes in the fracture of carbon nanotubes. *Chem. Phys. Lett.* 390, 413–420. doi:10.1016/j.cplett.2004.04.054

Mikata, Y. (2007). Complete solution of elastica for a clamped-hinged beam, and its applications to a carbon nanotube. *Acta Mech.* 190, 133–150. doi:10.1007/s00707-006-0402-z

Moser, J., Güttinger, J., Eichler, A., Esplandiu, M. J., Liu, D. E., Dykman, M. I., et al. (2013). Ultrasensitive force detection with a nanotube mechanical resonator. *Nat. Nanotechnol.* 8, 493–496. doi:10.1038/nnano.2013.97

Müller, Ralph H., and Petras, John F. (1938). A rapid method for traces of metals by the dropping mercury Electrode[1]. *J. Am. Chem. Soc.* 60, 2990–2993. doi:10.1021/ja01279a049

Nalaskowski, J., Niewiadomski, M., Paruchuri, V. K., and Miller, J. D. (2003). *Characterizatioin of spehrical alumina particles obtained by melting in a hydrogen-oxygen flame*. Littleton: Society for Mining, Mettalurgy, and Exploration.

Nguyen, C. V., Ye, Q., and Meyyappan, M. (2005). Carbon nanotube tips for scanning probe microscopy: Fabrication and high aspect ratio nanometrology. *Meas. Sci. Technol.* 16, 2138–2146. doi:10.1088/0957-0233/16/11/003

Nichol, J. M., Hemesath, E. R., Lauhon, L. J., and Budakian, R. (2008). Displacement detection of silicon nanowires by polarization-enhanced fiber-optic interferometry. *Appl. Phys. Lett.* 93, 193110. doi:10.1063/1.3025305

Nigmatullin, R., Lovitt, R., Wright, C., Linder, M., Nakari-Setälä, T., and Gama, M. (2004). Atomic force microscopy study of cellulose surface interaction controlled by cellulose binding domains. *Colloids Surfaces B Biointerfaces* 35, 125–135. doi:10.1016/j.colsurfb.2004.02.013

Oehrlein, G. S. (1989). Dry etching damage of silicon: A review. *Mater. Sci. Eng. B* 4, 441–450. doi:10.1016/0921-5107(89)90284-5

Ozin, G. A., and Arsenault, A. (2015). *Nanochemistry: A chemical approach to nanomaterials*. Cambridge, United Kingdom: Royal Society of Chemistry.

Pedersen, H. G., and Bergström, L. (1999). Forces measured between zirconia surfaces in poly(acrylic acid) solutions. *J. Am. Ceram. Soc.* 82, 1137–1145. doi:10.1111/j.1151-2916.1999.tb01887.x

Persson, B. N. J. (2007). Relation between interfacial separation and load: a general theory of contact mechanics. *Phys. Rev. Lett.* 99, 125502. doi:10.1103/PhysRevLett.99.125502

Poggio, M. (2013). Sensing from the bottom up. *Nat. Nanotechnol.* 8, 482–483. doi:10.1038/nnano.2013.124

Pu, D., and Hu, H. (2022). "Tip-based nanofabrication for NEMS devices," in *Advanced MEMS/NEMS fabrication and sensors*. Editor Z. Yang (Cham: Springer International Publishing), 1–18.

Rabinovich, Y. I., Adler, J. J., Ata, A., Singh, R. K., and Moudgil, B. M. (2000). Adhesion between nanoscale rough surfaces. *J. Colloid Interface Sci.* 232, 10–16. doi:10.1006/jcis.2000.7167

Raiteri, R., Preuss, M., Grattarola, M., and Butt, H.-J. (1998). Preliminary results on the electrostatic double-layer force between two surfaces with high surface potentials. *Colloids Surfaces A Physicochem. Eng. Aspects* 136, 191–197. doi:10.1016/S0927-7757(97)00339-7

Regan, M. J., Tostmann, H., Pershan, P. S., Magnussen, O. M., DiMasi, E., Ocko, B. M., et al. (1997). X-ray study of the oxidation of liquid-gallium surfaces. *Phys. Rev. B* 55, 10786–10790. doi:10.1103/physrevb.55.10786

Reiss, P., Protière, M., and Li, L. (2009). Core/shell semiconductor nanocrystals. *Small* 5, 154–168. doi:10.1002/smll.200800841

Roenbeck, M. R., Wei, X., Beese, A. M., Naraghi, M., Furmanchuk, A., Paci, J. T., et al. (2014). *In situ* scanning electron microscope peeling to quantify surface energy between multiwalled carbon nanotubes and graphene. *ACS Nano* 8, 124–138. doi:10.1021/nn402485n

Rossi, N., Braakman, F. R., Cadeddu, D., Vasyukov, D., Tütüncüoglu, G., Fontcuberta i Morral, A., et al. (2017). Vectorial scanning force microscopy using a nanowire sensor. *Nat. Nanotechnol.* 12, 150–155. doi:10.1038/nnano.2016.189

Roy, A., Mead, J. L., Wang, S., and Huang, H. (2017). Effects of surface defects on the mechanical properties of ZnO nanowires. *Sci. Rep.* 7, 9547. doi:10.1038/s41598-017-09843-5

Rumpf, H. (1974). Die wissenschaft des agglomerierens. *Chemie Ing. Techn.* 46, 1–11. doi:10.1002/cite.330460102

Sader, J. E., and Green, C. P. (2004). In-plane deformation of cantilever plates with applications to lateral force microscopy. *Rev. Sci. Instrum.* 75, 878–883. doi:10.1063/1.1667252

Savenko, A., Yildiz, I., Petersen, D. H., Bøggild, P., Bartenwerfer, M., Krohs, F., et al. (2013). Ultra-high aspect ratio replaceable AFM tips using deformation-suppressed focused ion beam milling. *Nanotechnology* 24, 465701. doi:10.1088/0957-4484/24/46/465701

Scharmann, F., Cherkashinin, G., Breternitz, V., Knedlik, C., Hartung, G., Weber, T., et al. (2004). Viscosity effect on GaInSn studied by XPS. *Surf. Interface Anal.* 36, 981–985. doi:10.1002/sia.1817

Schmutz, J.-E., Schäfer, M. M., and Hölscher, H. (2008). Colloid probes with increased tip height for higher sensitivity in friction force microscopy and less cantilever damping in dynamic force microscopy. *Rev. Sci. Instrum.* 79, 026103. doi:10.1063/1.2839020

Seo, M.-H., Yoo, J.-Y., Jo, M.-S., and Yoon, J.-B. (2020). Geometrically structured nanomaterials for nanosensors, NEMS, and nanosieves. *Adv. Mat.* 32, 1907082. doi:10.1002/adma.201907082

Shi, C., Luu, D. K., Yang, Q., Liu, J., Chen, J., Ru, C., et al. (2016). Recent advances in nanorobotic manipulation inside scanning electron microscopes. *Microsyst. Nanoeng.* 2, 16024. doi:10.1038/micronano.2016.24

Sobczak, Natalia, Sobczak, Jerzy, Asthana, Rajiv, and Purgert, Robert (2010). The mystery of molten metal. *China foundry* 7, 425–437.

Sqalli, O., Utke, I., Hoffmann, P., and Marquis-Weible, F. (2002). Gold elliptical nanoantennas as probes for near field optical microscopy. *J. Appl. Phys.* 92, 1078–1083. doi:10.1063/1.1487918

Stöber, W., Fink, A., and Bohn, E. (1968). Controlled growth of monodisperse silica spheres in the micron size range. *J. Colloid Interface Sci.* 26, 62–69. doi:10.1016/0021-9797(68)90272-5

Strus, M. C., Raman, A., Han, C. S., and Nguyen, C. V. (2005). Imaging artefacts in atomic force microscopy with carbon nanotube tips. *Nanotechnology* 16, 2482–2492. doi:10.1088/0957-4484/16/11/003

Strus, M. C., Zalamea, L., Raman, A., Pipes, R. B., Nguyen, C. V., and Stach, E. A. (2008). Peeling force spectroscopy: Exposing the adhesive nanomechanics of one-dimensional nanostructures. *Nano Lett.* 8, 544–550. doi:10.1021/nl0728118

Strus, M. C., Cano, C. I., Byron Pipes, R., Nguyen, C. V., and Raman, A. (2009). Interfacial energy between carbon nanotubes and polymers measured from nanoscale peel tests in the atomic force microscope. *Compos. Sci. Technol.* 69, 1580–1586. doi:10.1016/j.compscitech.2009.02.026

Sui, C., Luo, Q., He, X., Tong, L., Zhang, K., Zhang, Y., et al. (2016). A study of mechanical peeling behavior in a junction assembled by two individual carbon nanotubes. *Carbon* 107, 651–657. doi:10.1016/j.carbon.2016.06.069

Surmann, P., and Zeyat, H. (2005). Voltammetric analysis using a self-renewable non-mercury electrode. *Anal. Bioanal. Chem.* 383, 1009–1013. doi:10.1007/s00216-005-0069-7

Tabatabai, A., Fassler, A., Usiak, C., and Majidi, C. (2013). Liquid-phase gallium-indium alloy electronics with microcontact printing. *Langmuir* 29, 6194–6200. doi:10.1021/la401245d

Tabor, D. (1977). Surface forces and surface interactions. *J. Colloid Interface Sci.* 58, 2–13. doi:10.1016/0021-9797(77)90366-6

Tang, J., Zhao, X., Li, J., Guo, R., Zhou, Y., and Liu, J. (2017). Gallium-based liquid metal amalgams: Transitional-state metallic mixtures (TransM2ixes) with enhanced and tunable electrical, thermal, and mechanical properties. *ACS Appl. Mat. Interfaces* 9, 35977–35987. doi:10.1021/acsami.7b10256

Tevis, I. D., Newcomb, L. B., and Thuo, M. (2014). Synthesis of liquid core-shell particles and solid patchy multicomponent particles by shearing liquids into complex particles (SLICE). *Langmuir* 30, 14308–14313. doi:10.1021/la5035118

Thimons, L. A., Gujrati, A., Sanner, A., Pastewka, L., and Jacobs, T. D. B. (2021). Hard-material adhesion: Which scales of roughness matter? *Exp. Mech.* 61, 1109–1120. doi:10.1007/s11340-021-00733-6

Tsivion, D., Schvartzman, M., Popovitz-Biro, R., and Joselevich, E. (2012). Guided growth of horizontal ZnO nanowires with controlled orientations on flat and faceted sapphire surfaces. *ACS Nano* 6, 6433–6445. doi:10.1021/nn3020695

Vakarelski, I. U., and Higashitani, K. (2006). Single-nanoparticle-terminated tips for scanning probe microscopy. *Langmuir* 22, 2931–2934. doi:10.1021/la0528145

Wang, M. C. P., and Gates, B. D. (2009). Directed assembly of nanowires. *Mater. Today* 12, 34–43. doi:10.1016/S1369-7021(09)70158-0

Wang, C., and Madou, M. (2005). From MEMS to NEMS with carbon. *Biosens. Bioelectron.* 20, 2181–2187. doi:10.1016/j.bios.2004.09.034

Wang, S., Wu, Y., Lin, L., He, Y., and Huang, H. (2015). Fracture strain of SiC nanowires and direct evidence of electron-beam induced amorphisation in the strained nanowires. *Small* 11, 1672–1676. doi:10.1002/smll.201402202

Wang, S., Shan, Z., and Huang, H. (2017). The mechanical properties of nanowires. *Adv. Sci. (Weinh).* 4, 1600332. doi:10.1002/advs.201600332

Wang, S., Ma, L., Mead, J. L., Ju, S., Li, G., and Huang, H. (2021). Catalyst-free synthesis and mechanical characterization of TaC nanowires. *Sci. China Phys. Mech. Astron.* 64, 254612. doi:10.1007/s11433-020-1672-7

Wilson, N. R., and Macpherson, J. V. (2009). Carbon nanotube tips for atomic force microscopy. *Nat. Nanotechnol.* 4, 483–491. doi:10.1038/nnano.2009.154

Wong, S. S., Woolley, A. T., Odom, T. W., Huang, J.-L., Kim, P., Vezenov, D. V., et al. (1998). Single-walled carbon nanotube probes for high-resolution nanostructure imaging. *Appl. Phys. Lett.* 73, 3465–3467. doi:10.1063/1.122798

Xie, H., and Régnier, S. (2010). *In situ* peeling of one-dimensional nanostructures using a dual-probe nanotweezer. *Rev. Sci. Instrum.* 81, 035112. doi:10.1063/1.3360936

Xie, H., Mead, J. L., Wang, S., and Huang, H. (2017). The effect of surface texture on the kinetic friction of a nanowire on a substrate. *Sci. Rep.* 7, 44907. doi:10.1038/srep44907

Xie, H., Mead, J. L., Wang, S., Fatikow, S., and Huang, H. (2018a). Characterizing the surface forces between two individual nanowires using optical microscopy based nanomanipulation. *Nanotechnology* 29, 225705. doi:10.1088/1361-6528/aab3a5

Xie, H., Wang, S., and Huang, H. (2018b). Effects of surface roughness on the kinetic friction of SiC nanowires on SiN substrates. *Tribol. Lett.* 66, 15. doi:10.1007/s11249-017-0956-z

Yapici, M. K., and Zou, J. (2009). Microfabrication of colloidal scanning probes with controllable tip radii of curvature. *J. Micromech. Microeng.* 19, 105021. doi:10.1088/0960-1317/19/10/105021

Ye, Z., Lum, G. Z., Song, S., Rich, S., and Sitti, M. (2016). Phase change of gallium enables highly reversible and switchable adhesion. *Adv. Mat.* 28, 5088–5092. doi:10.1002/adma.201505754

Yerushalmi, R., Jacobson, Z. A., Ho, J. C., Fan, Z., and Javey, A. (2007). Large scale, highly ordered assembly of nanowire parallel arrays by differential roll printing. *Appl. Phys. Lett.* 91, 203104. doi:10.1063/1.2813618

Yibibulla, T., Mead, J. L., Ma, L., Hou, L., Huang, H., and Wang, S. (2022). The shearing behavior of nanowire contact pairs in air and the role of humidity. *Phys. Rapid Res. Ltrs.* doi:10.1002/pssr.202200130

Yuan, C. C., Zhang, D., and Gan, Y. (2017). Invited review article: Tip modification methods for tip-enhanced Raman spectroscopy (TERS) and colloidal probe technique: A 10 year update (2006-2016) review. *Rev. Sci. Instrum.* 88, 031101. doi:10.1063/1.4978929

Zhao, Y., Chen, X., Park, C., Fay, C. C., Stupkiewicz, S., and Ke, C. (2014). Mechanical deformations of boron nitride nanotubes in crossed junctions. *J. Appl. Phys.* 115, 164305. doi:10.1063/1.4872238

Zheng, M., and Ke, C. (2010). Elastic deformation of carbon-nanotube nanorings. *Small* 6, 1647–1655. doi:10.1002/smll.201000337

Zhou, O., Shimoda, H., Gao, B., Oh, S., Fleming, L., and Yue, G. (2002). Materials science of carbon nanotubes: Fabrication, integration, and properties of macroscopic structures of carbon nanotubes. *Acc. Chem. Res.* 35, 1045–1053. doi:10.1021/ar010162f

Zimmermann, S., and Huang, H. (2019). Investigating the effects of electron beam irradiation on nanoscale Adhesion. IEEE 14th International Conference on Nano/Micro Engineered and Molecular Systems, 33–38.

Zimmermann, S., Klauser, W., Mead, J., Wang, S., Huang, H., and Fatikow, S. (2019). A laterally sensitive colloidal probe for accurately measuring nanoscale adhesion of textured surfaces. *Nano Res.* 12, 389–396. doi:10.1007/s12274-018-2228-0

Zimmermann, S., Mead, J. L., and von Kleist-Retzow, F. T. (2020). Probing friction and adhesion of individual nanoplastic particles. *J. Phys. Chem. C* 124, 24145–24155. doi:10.1021/acs.jpcc.0c05826

Zuo, Y., Zheng, L., Zhao, C., and Liu, H. (2020). Micro-/Nanostructured interface for liquid manipulation and its applications. *Small* 16, e1903849. doi:10.1002/smll.201903849